Research Square

Preprints are preliminary reports that have not undergone peer review.
They should not be considered conclusive, used to inform clinical practice,
or referenced by the media as validated information.

Determination of Trunk Neural Crest Cell Fate and Susceptibility to Splicing Perturbation by the DLC1-SF3B1-PHF5A Splicing Complex

Zhengfan Zheng
School of Biomedical Sciences, Li Ka Shing Faculty of Medicine, The University of Hong Kong, Hong Kong, China

Suisui Guo
School of Biomedical Sciences, Li Ka Shing Faculty of Medicine, The University of Hong Kong, Hong Kong, China; Division of Life Science, The Hong Kong University of Science and Technology, Hong Kong, China

Yanxia Rao
School of Biomedical Sciences, Li Ka Shing Faculty of Medicine, The University of Hong Kong, Hong Kong, China; Shanghai Key Laboratory of Psychotic Disorders, Shanghai Mental Health Center, Shanghai Jiao Tong University School of Medicine, Shanghai 21108, China https://orcid.org/0000-0001-5292-2056

Man-Ning Hui
School of Biomedical Sciences, Li Ka Shing Faculty of Medicine, The University of Hong Kong, Hong Kong, China; Department of Obstetrics and Gynaecology, School of Clinical Medicine, Li Ka Shing Faculty of Medicine, The University of Hong Kong, Hong Kong, China

May Pui Lai Cheung
School of Biomedical Sciences, Li Ka Shing Faculty of Medicine, The University of Hong Kong, Hong Kong, China

Hoi Yau Tam
School of Biomedical Sciences, Li Ka Shing Faculty of Medicine, The University of Hong Kong, Hong Kong, China

Kelvin K. W. Wong
Centre for PanorOmic Sciences Proteomics and Metabolomics Core Facility, Li Ka Shing Faculty of Medicine, The University of Hong Kong, Hong Kong, China

Rakesh Sharma
Centre for PanorOmic Sciences Proteomics and Metabolomics Core Facility, Li Ka Shing Faculty of Medicine, The University of Hong Kong, Hong Kong, China

Jessica Aijia Liu
Department of Neuroscience, Tat Chee Avenue, City University of Hong Kong, Hong Kong, China

Martin Cheung

mcheung9@hku.hk

School of Biomedical Sciences, Li Ka Shing Faculty of Medicine, The University of Hong Kong, Hong Kong, China https://orcid.org/0000-0002-3471-8534

Article

Keywords:

Posted Date: May 10th, 2024

DOI: https://doi.org/10.21203/rs.3.rs-2603667/v1

License: This work is licensed under a Creative Commons Attribution 4.0 International License.
Read Full License

Additional Declarations:
There is **NO** Competing Interest.

Table 1 is available in the Supplementary Files section.

Version of Record: A version of this preprint was published at Nature Communications on July 21st, 2025. See the published version at https://doi.org/10.1038/s41467-025-62003-6.

Determination of Trunk Neural Crest Cell Fate and Susceptibility to Splicing Perturbation by the DLC1-SF3B1-PHF5A splicing complex

Zhengfan Zheng[1], Suisui Guo[1,2†], Yanxia Rao[1,3‡], Man-Ning Hui[1,4§], May Pui Lai Cheung[1], Hoi Yau Tam[1], Kelvin K.W. Wong[5], Rakesh Sharma[5], Jessica Aijia Liu[6] and Martin Cheung[1*]

[1]School of Biomedical Sciences, Li Ka Shing Faculty of Medicine, The University of Hong Kong, Hong Kong, China

[2†]Division of Life Science, The Hong Kong University of Science and Technology, Hong Kong, China

[3‡]Shanghai Key Laboratory of Psychotic Disorders, Shanghai Mental Health Center, Shanghai Jiao Tong University School of Medicine, Shanghai 21108, China

[4§]Department of Obstetrics and Gynaecology, School of Clinical Medicine, Li Ka Shing Faculty of Medicine, The University of Hong Kong, Hong Kong, China

[5]Centre for PanorOmic Sciences Proteomics and Metabolomics Core Facility, Li Ka Shing Faculty of Medicine, The University of Hong Kong, Hong Kong, China

[6]Department of Neuroscience, Tat Chee Avenue, City University of Hong Kong, Hong Kong, China

[†‡§]Present address

[*]Corresponding author: M.C. mcheung9@hku.hk

Abstract

Emerging evidence reveals the crucial role of ubiquitous splicing factors in neural crest (NC) development, which is highly susceptible to splicing dysregulation. How these factors integrate with the NC gene regulatory network (GRN) and contribute to the increased vulnerability of NC to splicing perturbations are not well understood. Here, we show that NC-specific DLC1, in association with the SF3B1-PHF5A splicing complex, are crucial for determining avian trunk NC cell fate by regulating the splicing of pre-mRNA for NC specifiers *SOX9* and *SNAI2* rather than their upstream regulators BMP4, WNT1, and PAX7 in the GRN. Mechanistically, SF3B1-PHF5A are associated with the branch point adenosine (BPA) of all the factors' introns, while DLC1 binds specifically to the BPA at the introns of *SOX9* and *SNAI2*, thereby determining the functional specificity of the SF3B1-PHF5A complex in NC specification. Moreover, DLC1 enhances the susceptibility of NC cells to the splicing modulator pladienolide B by reducing the binding capacity of the SF3B1-PHF5A splicing complex to the shorter length of both *SOX9* intron 2 and *SNAI2* intron 1, which have weaker polypyrimidine tract 3' of the BPA, resulting in intron retention and loss of NC progenitors. Our data highlight the critical role of the DLC1-SF3B1-PHF5A splicing complex in determining trunk NC cell fate and conferring its increased susceptibility to splicing perturbation.

Introduction

In vertebrates, multipotent neural crest cells (NCCs) are specified at the neural plate border between the neural plate and the non-neural ectoderm in the late gastrula stage of chick embryos [1]. Following neural tube closure, prospective NCCs in the dorsal neural tube undergo epithelial-mesenchymal transition (EMT) to acquire directional migratory behavior toward the periphery, where they give rise to the craniofacial structures and the peripheral nervous system [2]. Numerous studies have established a gene regulatory network (GRN) in which neural crest (NC) inductive signals (WNTs, BMPs, and FGFs) [3] cooperate with neural plate border specifiers (PAX7 and MSX1/2) to activate the transcription of NC specifier genes (*SOX9*, *SNAI2* and *FOXD3*) that determine NCC fate and EMT features [1, 4, 5, 6, 7]. Notably, *SOX9* and *SNAI2* are intron-containing genes that require additional underlying regulatory control of their pre-mRNA splicing to generate functional proteins. However, components of the spliceosome complex that regulate the pre-mRNA splicing of these NC specifiers remain largely unknown. In addition, genes encoding the spliceosome components are generally ubiquitously expressed, yet their mutations can lead to craniofacial malformations [8], suggesting a specific vulnerability of cranial NCCs to splicing abnormalities. Whether there is a similar susceptibility due to altered spliceosome components in trunk NCCs remains to be determined.

RNA splicing is a multi-step process regulated by the spliceosome, which comprises five small ribonucleoprotein particles (snRNPs) U1, U2, and U4/U5/U6 and their associated proteins unique to each snRNP [9]. Multi-RNAs and proteins are recruited and assembled on introns and then spliced by the stepwise recognition of the 5' splice site, the branch point adenosine (BPA) sequence, and the 3' splice site [10]. These processes produce reactive groups for intron excision and ligation of exons catalyzed by the spliceosome. A core component of U2 snRNP is SF3B1, the largest subunit comprising the SF3B complex, which plays a crucial role in BPA recognition at the 3' end of the

intron and promotes the stabilization of U2 and pre-mRNA in the early stages of spliceosome assembly [11]. In mouse embryos, SF3B1 is ubiquitously expressed but is more strongly expressed in the dorsal neural tube along the anterior-posterior axis [12]. Moreover, *SF3B1* null mutants die during preimplantation at around stage16-32 [13], indicating SF3B1 has an essential role in embryogenesis. Despite its broad expression, several reports have demonstrated that SF3B1 has specific functions in skeletal patterning [13], adult brain neurogenesis [14] and regulating the proliferative capacity of hematopoietic stem cells [15], indicating that SF3B1 has distinct regulatory roles in different cellular and tissue contexts. Consistently, hypomorphic *Sf3b1* mutant zebrafish embryos showed a marked reduction in the expression of a subset of trunk NC specifiers (e.g., sox9b, snail1b) partly due to aberrant processing of their pre-mRNAs, which led to defects in NC survival, migration, and lineage differentiation [16], suggesting that trunk NCCs are vulnerable to altered splicing machinery, yet the underlying mechanisms are not clear.

The PHD-finger domain protein 5A (PHF5A), a member of the PHD zinc finger superfamily, is a highly evolutionarily conserved splicing factor ubiquitously expressed in the nucleus of eukaryotes from yeast to humans [17]. It is intimately associated with SF3B1, SF3B3, and Sf3B5 involved in the formation of the core scaffolding in the SF3B complex of U2 snRNA protein [18]. Moreover, PHF5A serves as a bridge protein to facilitate interactions between U2 snRNA and ATP-dependent helicase in different phases of the splicing process [19, 20]. Structural analysis has revealed the interface between PHF5A and SF3B1 forms a pocket for BPA binding, which is the first critical step in the pre-mRNA splicing process [11, 21, 22]. Several small-molecule antitumor compounds have been identified to act as splicing modulators that bind the BPA pocket of the SF3B1-PHF5A complex in a competitive manner to disrupt the interaction with BPA [22, 23]. These compounds affect pre-mRNA splicing patterns in cells by triggering global exon skipping and intron retention depending on the sequence of the inhibited substrate, and the modulator structure, affinity and dose [24, 25]. Apart

from its involvement in splicing, PHF5A can function as a transcription factor regulating the expression of connexin43 gene in response to estrogen [26], modulating stem cell features in pancreatic cancer cells [27], and maintaining the pluripotency of embryonic stem cells (ESCs) [28]. Given that SF3B1 is required for NC specification via regulating the splicing of NC specifiers and that PHF5A regulates the pluripotency of ESCs, it is plausible that PHF5A is associated with SF3B1 in regulating the formation of multipotent NC stem cells at the transcriptional and/or post-transcriptional level.

Here, we employed CRISPR-Cas9 genome editing approach in avian embryos to show that NC-specific DLC1, in association with the ubiquitously expressed SF3B1-PHF5A complex, is required for trunk NCC fate determination via regulating the pre-mRNA splicing of NC specifiers *SOX9* and *SNAI2* rather than their upstream regulators BMP4, WNT1, and PAX7. RNA immunoprecipitation demonstrated the specific binding of endogenous DLC1 to the BPA of *SOX9* and *SNAI2* introns, which controls the splicing specificity of the SF3B1-PHF5A complex in NC specification. Treatment with the splicing modulator pladienolide B (PB) in ovo inhibited BPA recognition by SF3B1-PHF5A, leading to the loss of SOX9 and SNAI2 expression in trunk NCCs. However, their expression remained unchanged in somites that do not express DLC1. Mechanistically, DLC1 weakened the binding capacity of the SF3B1-PHF5A splicing complex to the shorter length of both *SOX9* intron 2 and *SNAI2* intron 1, which exhibit a weaker Polypyrimidine (Py)-tract than in *SOX9* intron 1 and *SNAI2* intron 3. This explains the heightened susceptibility of NCCs to PB, resulting in intron retention and loss of NC progenitors. Overall, our findings demonstrate that an NC-specific DLC1-SF3B1-PHF5A splicing complex plays a crucial role in specifying trunk NCC fate and conferring its increased susceptibility to splicing perturbation.

Results

DLC1 is required for pre-mRNA splicing of SOX9 and SNAI2 introns

Our previous studies have shown that *DLC1* is expressed in early delaminating and emigrating trunk NCCs from Hamburger and Hamilton (HH) stages (st) 11 to 13 of chick embryo development, consistent with its role in governing directional delamination and migration [29]. However, a reexamination of *DLC1* expression at the trunk level of st 10 chick embryo revealed co-expression with *SOX9* and *SNAI2* in the premigratory NC region where progenitors reside (Fig. 1a), suggesting a potential role for DLC1 in NC specification. To investigate this further, we used CRISPR/Cas9 genome editing to knockout (KO) *DLC1* in developing chick neural tubes. Two different guided RNA (gRNA) oligos were designed to target *DLC1* exon 9 (*DLC1 gRNA1* and *gRNA2*) (Fig. 1b) and a non-targeting gRNA served as a control (Ctrl). Each gRNA or control (Ctrl) gRNA was co-electroporated with a construct encoding nuclear Cas9 and GFP into the right side of the avian trunk neural tube at st 9-10 [30] when NC specification begins (Fig. 1c). At 9 hours post-transfection (hpt), both *gRNAs* significantly reduced DLC1 protein expression compared to the *Ctrl gRNA* (Fig. 1d). We present the results of *DLC1 gRNA1* unless otherwise stated, as similar findings were observed with both gRNAs. Electroporation of *DLC1 gRNA1* led to cell-autonomous reductions in the expression of *SOX9*, *SNAI2,* and *FOXD3* in the pre-migratory NC domain compared to the *Ctrl gRNA* (Fig. 1e). Fluorescence-activated cell sorting of transfected cells for qPCR analysis further confirmed reduction of their mRNA levels (Fig. 1f-h). Importantly, the reintroduction of full-length DLC1, rather than its individual SAM or RhoGAP domains, was sufficient to restore the decreased expression of *SOX9*, *SNAI2,* and *FOXD3* caused by *DLC1 gRNA1* (Fig. 1e, Fig. S1a), highlighting the specificity of *DLC1 KO* and the RhoGAP independent activity of DLC1. In addition, we observed the nuclear localization of ectopic DLC1 (Fig. 1i), indicating its potential involvement in gene expression regulation. Immunofluorescence staining

revealed a loss of SOX9 expression in the dorsal neural tube transfected with *DLC1 gRNA1*, while the expression of neural stem/progenitor marker SOX2 was upregulated (Fig. 1j), suggesting a switch in cell fate from NC to neural lineage. This was accompanied by a significant reduction in migratory NCCs expressing HNK-1 (Fig. 1k). Importantly, the levels of NC inductive signals *WNT1*, *BMP4,* and the expression of neural plate border gene *PAX7* were unaffected by *DLC1 gRNA1* and *gRNA2*, indicating that the decrease in expression of NC specifier genes was not due to alterations in the expression of their upstream regulators in the GRN (Fig. S1b-e). Additionally, the levels of RNA polymerase II phosphorylation at Ser 5 (PolII-pSer5) and Ser 2 (PolII-pSer2), which are involved in transcription initiation and elongation[31], respectively, were not significantly affected by *DLC1 gRNA1* and *gRNA2* (Fig. 1l). To investigate whether DLC1 regulates transcriptional elongation of NC specifier genes, chromatin immunoprecipitation of PolII-pSer2 was performed at multiple sites along the *SOX9* and *SNAI2* genomic DNA in embryos treated with *DLC1 gRNA1* or *Ctrl gRNA*. We detected a 4-fold enrichment of PolII-pSer2 at the 500 bp downstream of the *SOX9* transcriptional start site in cells transfected *DLC1 gRNA1* compared to those transfected with Ctrl gRNA. However, the enrichment was reduced to a level similar to the Ctrl gRNA from 1000 bp onwards to the end of the *SOX9* gene body (Fig. S1f). There is no significant difference in the degree of PolII-pSer2 association with *SNAI2* genomic DNA at different sites between *DLC1 gRNA1* and *Ctrl gRNA* (Fig. S1g), indicating that transcriptional elongation still occurs in the absence of DLC1. These findings suggest that DLC1 is not directly involved in transcriptional regulation. Instead, intron retention analysis revealed increased levels of *SOX9* introns 1 and 2 in *DLC1 KO* transfected cells compared to the *Ctrl gRNA* (Fig. 1m, n). Similar results were observed for *SNAI2* introns 1 and 3, although intron 2 was too short for detection (Fig. 1o, p). Hybridization chain reaction (HCR) analysis was able to detect the intron-retained *SOX9* and *SNAI2* mRNAs in the dorsal neural tubes transfected with *DLC1 gRNA1* (Fig.

1q). These results suggest that the downregulated expression of *SOX9* and *SNAI2* in response to *DLC1 KO* may be attributed to the dysregulated splicing process of their pre-mRNAs. Considering that SOX9 regulates *FOXD3* expression [6], the loss of *FOXD3* expression in *DLC1 KO* cells may be due to the depletion of $SOX9^+$ NC progenitors. Taken together, these findings suggest that DLC1 is required for NC specification by regulating pre-mRNA splicing of *SOX9* and *SNAI2*.

DLC1 associates with the PHF5A-SF3B1 splicing complex which is required for pre-mRNA splicing of SOX9 and SNAI2 introns

To elucidate the molecular mechanism by which DLC1 regulates gene splicing, we conducted mass spectrometry (MS) analysis on DLC1-immunoprecipitated lysates from chick neural tubes to identify interacting factors of DLC1. Among the many DLC1-1 interacting factors involved in diverse molecular functions, one of the major categories is RNA binding proteins, which mainly consist of splicing factors (Fig. S2a). This category includes PHF5A and SF3B1, both of which are components of the SF3B complex within the U2 snRNP spliceosome involved in pre-mRNA splicing[32] (Fig. 2a, Dataset S1). Immunoprecipitation experiments confirmed the association of endogenous DLC1 with PHF5A and SF3B1 (Fig. 2a). Consistently, MS analysis of PHF5A-immunoprecipitated lysates from chick neural tubes demonstrated the existence of the endogenous PHF5A-SF3B1 complex (Fig. 2b, Dataset S2), and their interaction was further confirmed by immunoprecipitation (Fig. 2b). Additionally, we detected co-localization of the ubiquitously expressed PHF5A-SF3B1 complex with DLC1 in the premigratory NCCs (Fig. S2b). The ability of DLC1 to interact with the PHF5A-SF3B1 splicing complex raises the possibility that PHF5A-SF3B1 could be involved in NC specification. To investigate this hypothesis, we employed a similar CRISPR/Cas9 genome editing approach to KO *PHF5A* in developing chick neural tubes using two gRNA oligos targeting exons 3 and 4 of *PHF5A* (*gRNA1*, *gRNA2*) (Fig. 2c). After 8 hpt,

we observed a significant reduction of PHF5A expression in gRNA-transfected cells compared to the Ctrl gRNA (Fig. 2c), confirming successful *PHF5A KO*. For subsequent studies, we utilized *gRNA1* as similar results were obtained with *gRNA2*. Electroporation of *PHF5A gRNA1* resulted in cell-autonomous downregulation of *SOX9*, *SNAI2*, and *FOXD3* expression in the premigratory NC region, as confirmed by qPCR analysis of sorted cells when compared to the unaltered expressions observed in *Ctrl gRNA* and the untransfected side (Fig. 2d-i). Co-expression of *PHF5A gRNA1*/Cas9 constructs with a vector encoding full-length chick *PHF5A* cDNA, rather than the PHD domain alone, restored the expression of NC specifier genes (Fig. 2d, f, h and Fig. S2c), demonstrating the specificity of *PHF5A KO*. Consistent with the downregulation of NC specifiers, the domain of SOX2 expression expanded into the NC territory, where SOX9 was diminished (Fig. 2j), indicating a switch in cell fate from NC to neural progenitors. Similar to the results observed with *DLC1 KO*, *PHF5A gRNA* did not alter the expression levels of *WNT1*, *BMP4,* and PAX7 (Fig. S2d-g). The loss of NC progenitors in *PHF5A KO* embryos resulted in a lack of migratory NCCs expressing HNK-1 (Fig. 2k). As PHF5A has been implicated in the control of transcriptional elongation of genes that maintain pluripotency in ESCs [28], we investigated whether PHF5A associates with PolII to regulate the transcription of NC specifier genes. Immunoprecipitation experiments revealed that PHF5A did not interact with PolII-pSer5 or PolII-pSer2 (Fig. S2h, i) [31]. Despite the efficient *KO* of *PHF5A*, the levels of PolII-pSer5 and PolII-pSer2 remained largely unchanged (Fig. 2l), indicating that the loss of NC specifier gene expression following *PHF5A KO* is not due to altered levels of the transcriptional machinery. Instead, *PHF5A gRNA1* led to increased levels of introns 1 and 2 of *SOX9*, and introns 1 and 3 of *SNAI2*, when compared to the *Ctrl gRNA* (Fig. 2m-p). HCR analysis detected the expression of these introns in *PHF5A KO* embryos but not in *Ctrl gRNA*-treated embryos (Fig. 2q). Similarly, *SF3B1 KO* resulted in a loss of NC progenitors due to intron retention of *SOX9* and *SNAI2* pre-mRNA without altering the

expression of their upstream regulators and transcriptional machinery (Fig. S3a-p). Importantly, *PHF5A KO* and *SF3B1 KO* did not affect the expression levels of *SF3B1* or *PHF5A*, respectively (Fig. S3q, r), indicating they do not regulate the expression of each other to determine NCC fate. To further confirm the splicing defects in each KO, we conducted RT-PCR with specific primers to examine the levels of unspliced and spliced forms of each intron (Fig. S4a, b). The use of two different gRNAs targeting *PHF5A*, *SF3B1,* and *DLC1* genes resulted in increased ratios of unspliced transcripts to varying degrees for each intron of *SOX9* and *SNAI2* when compared to the *gRNA* Ctrl (Fig. S4c-j). Conversely, the unspliced forms of *PAX7*, *BMP4,* and *WNT1* were not predominantly expressed in all KO treatments and Ctrl gRNA, except for *BMP4 intron 2* which did not show a discernible difference in the ratio of unspliced and spliced counts between each KO and *Ctrl gRNA* (Fig. S5a-f). These findings are consistent with the unaltered mRNA levels of *BMP4, WNT1*, and PAX7 when *DLC1*, *PHF5A*, or *SF3B1* are absent (Fig. S1b-e; S2d-g; S3g-j). Additionally, RT-PCR analysis indicated that there was no exon skipping of *SOX9* and *SNAI2* in any of the KO treatments (Fig. S6a-d), suggesting that the decreased expression of *SOX9* and *SNAI2* mRNA in all KO treatments is primarily due to intron retention. In agreement with this, transcriptomic profiling of sorted GFP+ cells from embryos treated with each gRNA confirmed increased intron depth for *SOX9* and *SNAI2* relative to *Ctrl gRNA* (Fig. 3a-d). Additionally, other neural crest specifier genes (*ID1*, *TWIST1*, and *MYC*) also showed different levels of intron retention in each gRNA treatment (Fig. 3e-g). In contrast, the levels of retained introns for *PAX7*, *BMP4, WNT1,* and another neural plate border marker MYB were low or comparable in all treatment groups (Fig. 3h-n, Dataset S3). Collectively, these findings suggest that nuclear DLC1 associated with the PHF5A-SF3B1 splicing complex has a specific role in NC determination by regulating the splicing of *SOX9* and *SNAI2* pre-mRNA and other NC specifier genes.

DLC1 determines the functional specificity of the PHF5A-SF3B1 splicing complex in NC specification through binding to the BPA in SOX9 and SNAI2 introns

Since the DLC1-PHF5A-SF3B1 complex regulates gene splicing, we then examined whether they could bind to the BPA within *SOX9* and *SNAI2* introns in chick neural tubes. To this end, we performed RNA immunoprecipitation (RIP)-qPCR to determine the ability of each endogenous protein to associate with BPA in each intron. We incubated lysates generated from wild-type HH9-10 embryonic trunks with magnetic beads coated with DLC1, PHF5A, SF3B1, or IgG non-specific control antibodies. The eluted RNA from the beads was subjected to qRT-PCR with primers flanking the BPA in each intron (Fig. 4a, b). We found the BPA of each intron was significantly enriched by DLC1, PHF5A, and SF3B1 antibodies compared to IgG (Fig. 4c-h), confirming their intronic binding capacity. Further investigation was carried out to determine whether DLC1 is essential for the association of PHF5A-SF3B1 complex and/or their binding to the BPA of *SOX9* and *SNAI2* introns. Immunoprecipitation and RIP-qPCR were performed for PHF5A and SF3B1 in embryos treated with *DLC1 gRNA1*. The results revealed that *DLC1 KO* did not disrupt the interaction between SF3B1 and PHF5A1 (Fig. 4i), but significantly reduced the enrichment of PHF5A and SF3B1 at the BPA of *SOX9* and *SNAI2* introns compared to *Ctrl gRNA* (Fig. 4j-m). These results suggest that DLC1 is necessary for the binding capacity of the PHF5A-SF3B1 complex to these introns, providing a mechanistic explanation for the lack of NC progenitors formation resulting from the loss of DLC1 function due to defective binding of the PHF5A-SF3B1 complex to *SOX9* and *SNAI2* introns at the BPA for splicing initiation. We next examined whether PHF5A, SF3B1, and DLC1 could bind to the BPA of the introns of *PAX7*, *WNT1,* or *BMP4* pre-mRNAs. While the PHF5A-SF3B1 complex remained strongly associated with the BPA of each gene intron (Fig. S7a-f), DLC1 did not bind to any of them (Fig. S7g-i). Consistently, *DLC1 KO* did not disrupt the binding capacity of the PHF5A-SF3B1 complex to the BPA of the introns of

WNT1, *BMP4,* or *PAX7* (Fig. S7j-u). Altogether, these findings suggest that the ability of DLC1 to associate with the BPA of *SOX9* and *SNAI2* introns determines the functional specificity of PHF5A-SF3B1 in NC specification.

Splicing modulator specifically abolishes NC specifier gene expression

To further investigate the role of the PHF5A-SF3B1 complex in regulating the splicing of *SOX9* and *SNAI2* pre-mRNAs by binding to BPA, we treated HH10 avian trunk neural tubes at the thoracic level with the splicing modulator pladienolide B (PB), which is cytotoxic to cancer cells [22, 33]. PB is known to disrupt the interaction between the PHF5A-SF3B1 complex and BPA, leading to impaired mRNA splicing [23, 24, 33]. After a 5-hour treatment with 200 μM PB, we performed *in situ* hybridization with NC specifier genes on harvested embryos (Fig. 5a). Transverse sections of the stained embryos revealed a complete loss of *SOX9*, *SNAI2,* and *FOXD3* expression in the premigratory NC region compared to control embryos treated with PBS (Fig. 5b). Intriguingly, expression of *SOX9* and *SNAI2* in somites remained unchanged (Fig. 5b), suggesting that trunk NCCs are more susceptible to PB treatment. The loss of SOX9 and SNAI2 expression was not due to reduced expression of neural plate border specifier or cell death, as evidenced by the unchanged expression of PAX7 and the absence of Caspase-3 in PB-treated embryos (Fig 5c, d). Furthermore, PB treatment did not affect the expression levels of DLC1, PHF5A, SF3B1, or PolII (Fig. 5d), nor did it disrupt the interactions between DLC1 and SF3B1 or between PHF5A and SF3B1 (Fig. 5e). The finding supports the proposed mechanism of PB action, which targets the binding capacity of PHF5A-SF3B1 to BPA without affecting transcriptional expression and protein-protein interactions. qPCR analysis revealed that PB treatment specifically retained intron 2 of *SOX9* and intron 1 of *SNAI2* (Fig. 5f-i). This was further confirmed by the detection of the HCR signal for these introns in premigratory and early migratory NCCs. In contrast, there was no HCR signal for

intron 1 of *SOX9* and intron 3 of *SNAI2* (Fig. 5j-n). This difference is likely attributed to the shorter length of *SOX9* intron 2 and *SNAI2* intron 1, which have a weaker polypyrimidine (Py) tract located at the 3' end of BPA compared to *SOX9* intron 1 and *SNAI2* intron 3 (Table 1). Consequently, the binding of PHF5A-SF3B1 to BPA is disrupted upon PB treatment [22, 24]. Indeed, RIP assay revealed that PB treatment reduced the binding capacity of PHF5A-SF3B1 to *SOX9* intron 2 and *SNAI2* intron 1 but did not alter their ability to bind to *SOX9* intron 1 and *SNAI2* intron 3 compared to the PBS control (Fig. 5o-r). No exon skipping was detected in *SOX9* and *SNAI2* after PB treatment (Fig. S6b, d). Overall, these findings demonstrate that PB treatment specifically abolished the expression of NC specifier genes, likely through competitive inhibition of the recognition of BPA in *SOX9* intron 2 and *SNAI2* intron 1 by the PHF5A-SF3B1 complex.

DLC1 determines the increased vulnerability of trunk NCCs to PB treatment.

The lack of an effect of PB on *SOX9* and *SNAI2* expression in somites may be attributed to the absence of NC-specific splicing factors associating with the PHF5A-SF3B1 complex that confer increased susceptibility to trunk NCCs by interfering with BPA recognition via the complex following PB treatment. Based on the aforementioned results, we hypothesize that DLC1 may serve as an NC-specific splicing factor that determines trunk NCC vulnerability to a splicing modulator, as it was absent in somites and might explain the observed resistance of somites while the increased susceptibility of NCCs to PB treatment (Fig. 1a, S2b) To test this hypothesis, we electroporated the full-length *DLC1* cDNA construct into somites at HH10 and incubated for 8 h before treating with PB or PBS control for 5 hours (Fig. 6a). The results showed that the ectopic DLC1 did not affect SOX9 and SNAI2 expression in both NCCs and somites of embryos treated with PBS. In contrast, PB treatment led to the loss of SOX9 and SNAI2 expression in DLC1-overexpressing somites in a cell-autonomous manner (Fig 6b-e). Immunoprecipitation using chick embryo lysates

revealed that ectopic DLC1 was still able to interact with endogenous PHF5A and SF3B1 in somites following PB treatment (Fig. 6f), which is consistent with its nuclear localization (Fig. S8a). Intron retention analysis in sorted somites electroporated with *DLC1* showed increased levels of *SOX9* intron 2 and *SNAI2* intron 1 as what was observed in NCCs following PB treatment (Fig. 6g-j). In agreement with this, HCR analysis showed the expression of *SOX9 intron 2* and *SNAI2 intron 1* in DLC1-transfected somites, whereas the expression of *SOX9 intron 1* and *SNAI2 intron 3* was not detected (Fig. 6k-o) The RIP assay further showed that electroporation of DLC1 into somites of embryos treated with PB led to a marked reduction in the binding capacity of PHF5A and SF3B1 to both *SOX9* intron 2 and *SNAI2* intron 1 compared to the PBS control (Fig. 7a-d). This suggests that the overexpression of DLC1 specifically weakened the interaction of the PHF5A-SF3B1 complex with the BPA of *SOX9* intron 2 and *SNAI2* intron 1, which are shorter and have a lower Py-tract score compared to *SOX9* intron 1 and *SNAI2* intron 3, respectively (Table 1). Indeed, protein binding assay using in vitro translated DLC1, PHF5A, and SF3B1 proteins further confirmed the lack of association of DLC1-PHF5A-SF3B1 complex with *SOX9 intron 2* and *SNAI2 intron 1* in the presence of PB but not PBS control (Fig 7e). These findings indicate that NC-specific DLC1 plays a crucial role in conferring increased vulnerability of trunk NCCs to splicing perturbation.

Discussion

The formation of NCCs is regulated by a gene regulatory network in various vertebrate species. This network involves signaling pathways, such as WNT1 and BMP4, which activate the expression of transcription factors like PAX7 to establish the neural plate border. These signaling effectors, along with regulators of the neural plate border, then activate the expression of NC specifiers including SOX9, SNAI2, and FOXD3, which determine the fate of multipotent NCC

progenitors. However, the factors involved in regulating the splicing of intron-containing *SOX9* and *SNAI2* genes have not been identified. In this study, we investigated the role of SF3B1-PHF5A spliceosome component in conjunction with NCC-specific factor DLC1 in avian trunk NC specification. We demonstrated that these factors are functionally important for NCC formation by regulating the splicing of *SOX9* and *SNAI2* pre-mRNA, but not their upstream regulators BMP4, WNT1, and PAX7. Mechanistically, the binding ability of DLC1 at the BPA in *SOX9* and *SNAI2* introns determines the splicing specificity of SF3B1-PHF5A in NCC specification. Treatment with the splicing modulator PB in ovo blocked the recognition of BPA by SF3B1-PHF5A, leading to the loss of SOX9 and SNAI2 expression specifically in trunk NCCs, but not in somites. Furthermore, we demonstrated that DLC1 enhances the vulnerability of trunk NCCs to PB treatment by reducing the binding capacity of SF3B1-PHF5A to both *SOX9* intron 2 and *SNAI2* intron 1, which are shorter in length and have a weaker Py-tract compared to *SOX9* intron 1 and *SNAI2* intron 3. Collectively, our findings reveal that the DLC1-SF3B1-PHF5A splicing complex, specific to NCCs, plays a critical role in determining NCC fate and confers increased vulnerability to splicing perturbations (Fig. 7f).

Splicing is considered to be an essential ubiquitous process that involves excision of introns to form mature RNA, which also increases the diversity of proteins generated from the genome [34]. The spliceosome component SF3B1 is the largest subunit within the SF3B complex of the U2 snRNP. It is mainly involved in the recognition of BPA to promote the stable interaction of U2 with pre-mRNA in the initial phase of the splicing process [11]. Another splicing factor PHF5A closely associated with SF3B1 is important for both spliceosome structural stability, and for linking the spliceosome to histones [22, 35]. Structural analysis has shown that the interface between SF3B1 and PHF5A forms a pocket for BPA binding [36]. We have confirmed the endogenous interactions between SF3B1 and PHF5A, and showed they bind to BPA close to the 3’ splicing sites of *SOX9*

and *SNAI2* introns in chick embryos. Consistently, CRISPR/Cas9-mediated knockout of *PHF5A* or *SF3B1* led to the loss of *SOX9* and *SNAI2* mRNA expression due to splicing perturbations, resulting in intron retention. These aberrantly spliced mRNAs are likely degraded by nonsense-mediated mRNA decay to inhibit the generation of truncated proteins that are harmful to cells [37]. Our results are in line with previous studies that showed Sf3b1 is required for trunk NCC specification in zebrafish embryos [16], suggesting the function of Sf3B1 is conserved between chick and zebrafish embryos. As *Sf3b1* null mutants die during preimplantation [13], generation of *Sf3b1* conditional mutants crossed with NC-specific Cre transgenic line would be warranted to determine whether mouse Sf3b1 also plays a role in NC formation similar to in chick and zebrafish embryos. In addition, SF3B1 and PHF5A do not regulate the expression of each other, ruling out a regulatory relationship in NC specification. The retained introns for *SOX9* and *SNAI2* mRNA likely involve the lack of binding capacity of SF3B1 and PHF5A to BPA in *PHF5A KO* and *SF3B1 KO*, respectively, which disrupts the assembly and stability of U2-dependent spliceosome for subsequent splicing events, as demonstrated in other studies [22, 35]. Consistent with this notion, overexpression of full-length *PHF5A* cDNA was able to restore the expression of NC specifier in *PHF5A KO* embryos, possibly via the restoration of SF3B1-PHF5A splicing complex formation and binding to BPA. Our results support the importance of this complex for gene splicing *in vivo*. Although PHF5A has been shown to regulate PolII elongation in genes that are essential for maintaining pluripotency of ESCs [28], we found PHF5A did not associate with PolII-pSer5 and PolII-pSer2, as *PHF5A KO* did not affect their expression, which excludes a transcriptional role of PHF5A in regulating NC formation. However, previous studies showed that PHF5A functions as a transcription factor regulating genes that contribute to the stemness of cancer cells [27, 38], which highlights the functional importance of PHF5A in regulating stem cell features in both developmental and pathological contexts. Whether PHF5A functions as a transcription factor or

splicing factor in regulating the expression of genes that are essential for the formation of other tissue progenitors and maintaining the stemness of other types of cancer stem cells remains to be determined.

Our previous studies showed that the asymmetric localization of cytoplasmic DLC1 functions as a RhoGAP to establish differential RHOA activity at the cell rear and front edge that controls trunk NCC polarity for directional delamination and migration [29]. In contrast, the current study revealed an unprecedented role of nuclear DLC1 in trunk NCC fate determination through the association with SF3B1-PHF5A complex to regulate splicing of *SOX9* and *SNAI2* pre-mRNA. These studies also reveal the spatio-temporal requirement of DLC1 in regulating NC specification and migration, as *DLC1 KO* at HH9-10 reduced NC formation whereas knockdown in committed NCCs at HH11-12 disrupted their migration directionality [29]. The underlying mechanisms to controlling DLC1 translocation from the nucleus to the cytoplasm as prospective NCCs undergo delamination remains to be determined. Previously, we showed nuclear DLC1 can associate with FOXK1 transcription factor to cooperatively activate MMP9 expression in promoting melanoma metastasis [39]. It is conceivable that nuclear DLC1 is an important regulator that controls various developmental and pathological processes at the transcriptional and/or post-transcriptional levels.

Our study provides evidence of the involvement of DLC1 in the splicing process: 1) nuclear DLC1 can interact with the SF3B1-PHF5A splicing complex, 2) DLC1 binds to the BPA of *SOX9* and *SNAI2* introns, 3) DLC1 is required for the SF3B1-PHF5A splicing complex to bind to the BPA of *SOX9* and *SNAI2* introns, and 4) *DLC1 KO* leads to retention of *SOX9* and *SNAI2* intron transcripts without affecting the expression and function of their transcriptional machinery. However, DLC1 does not bind to the BPA of *WNT1*, *BMP4*, or *PAX7* introns, which might explain the lack of impact on BPA recognition by the SF3B1-PHF5A complex and splicing of *WNT1*, *BMP4*, and *PAX7* introns in the absence of DLC1. These findings suggest that differences in the

sequences flanking the BPA may determine the binding specificity of DLC1 and its association with the SF3B1-PHF5A complex in regulating the splicing of gene subsets. Based on this notion, certain splicing complexes containing SF3B1-PHF5A together with cell-type- or stage-specific factors may be needed to bind BPA and regulate the splicing of *WNT1*, *BMP4*, and *PAX7* introns. The identity of these factors has yet to be identified. Previous single-cell transcriptomic studies have indicated that multipotent NC formation is subject to multiple waves of transcriptomic changes, which are likely accompanied by increased levels of alternative splicing and translation to efficiently generate numerous and distinct cell types over a relatively short period [40, 41]. Thus, an increased splicing requirement of the formation of NC progenitors may contribute to their increased susceptibility to reduced levels of splicing factors. Such a requirement may explain why the KO of *PHF5A* or *SF3B1* only caused splicing defects in NC specifier genes instead of their upstream regulators. In agreement with this, functional perturbations of several core splicing factors lead to defects in cranial NC formation [42]. In addition, distinct components of the splicing complex in different cellular contexts may determine the degree of vulnerability to splicing perturbations. Our *in ovo* experiment demonstrated that PB treatment resulted in the loss of SOX9 and SNAI2 expression in NCCs, but not in somites. This is due to NC-specific DLC1 that appears to weaken the binding affinity of the SF3B1-PHF5A complex to both *SOX9* intron 2 and *SNAI2* intron 1, likely due to their shorter length and weaker Py-tracts compared to *SOX9* intron 1 and *SNAI2* intron 3. Previous findings showed that shorter introns with weaker Py-tracts were more prone to being retained upon inhibition of SF3B1 and PHF5A activity [24]. This was further supported by the overexpression of DLC1 in somites, which resulted in the loss of SOX9 and SNAI2 expression in the presence of PB due to the retention of *SOX9* intron 2 and *SNAI2* intron 1. These findings raise the intriguing possibility of a specific splicing complex that regulates the splicing of *SOX9* and *SNAI2* pre-mRNAs in somites and is more resistant to splicing perturbation.

Previous studies have reported that mutations in the core components of the spliceosome lead to craniofacial disorders [8]. Most of these defects occur at the levels of NC formation, migration, and differentiation to skeletal lineages. For example, *sf3b4* knockdown in *Xenopus* embryos resulted in the disruption of cranial NC formation, which reduced their migratory capacity and differentiation potency toward skeletal elements in the cranial region [43]. In contrast, *Sf3b1* knockdown in zebrafish embryos showed defects in trunk NC formation without affecting cranial NC development [16]. Whether distinct complexes orchestrate the splicing of genes essential for cranial and trunk NC development in different vertebrate species remains to be elucidated. Nevertheless, our studies suggest that the splicing complexes in cranial NCCs may contain cell-type- or gene-specific factors that contribute to their increased susceptibility to reduced levels, function, or intron binding capacity of splicing factors. Identification of these factors should provide mechanistic insights into how mutations in ubiquitously expressed spliceosome components can lead to craniofacial abnormalities.

Methods

Chick embryos and in ovo electroporation

Fertilized chick Leghorn eggs were purchased by Jinan Poultry Co. China through Tin Hang Technology Ltd and incubated at 38.5°C in a humidified incubator. Embryos were staged according to Hamburger and Hamiliton (HH) stages [30]. All animal experiments were approved by the Committee on the Use of Live Animals in Teaching and Research, The University of Hong Kong (CULATR No: 5969-21). *In ovo* electroporation was performed as described previously [44]. Plasmid DNA (3 μg/μL) or gRNAs/Cas9 (Cas9 2 μg/μL + gRNA 1.5 μg/μL) constructs were injected into the lumen of closed neural tubes or the cavity of somites of embryos at HH9-10 using a glass capillary. Electrodes were placed on either side of the neural tube or somites, and electroporation was carried out using a BTX electroporator delivered as five 50 ms pulses, 450- ms interval at 36

V. Electroporated embryos were allowed to develop for 8 h post-transfection (hpt) before being processed for fluorescence activated cell sorting (FACS) for genotyping analysis, Western blotting, immunofluorescence, whole mount *in situ* hybridization, immunoprecipitation, RNA-immunoprecipitation (RIP)-qPCR, intron retention analysis and RNA-sequencing (RNA-seq). Wild-type HH10 or electroporated embryos 8 hpt were treated with PB (200 μM) before being processed for *in situ* hybridization, intron retention analysis and RIP-qPCR.

Plasmid construction

Full-length chick *PHF5A cDNA* (NM_001277376.2*)*, PHD domain, *DLC1 cDNA* [29], SAM domain and RhoGAP domain were inserted at the *Xho1* and *Cla1* sites upstream of an internal ribosomal entry site (IRES) followed by a tdTomato cDNA in a pCIG expression vector (kind gift of A. McMahon, University of Southern California, USA). Three plasmids for CRISPR/Cas9 KO in chick embryos (U6.3>gRNA.f+e, #99139, U6.3>Control.gRNA (GCACTGCTACGATCTACACC). f+e, #99140, pCAGG nls-hCas9-nls-GFP, #99141) were purchased from Addgene. Online program E-CRISP was used for gRNA design. gRNA oligos were synthesized by Integrated DNA technologies (IDT) and cloned into U6.3 gRNA.f+e vector (Table S1).

FACS and genotyping

The electroporated embryos were harvested 8 hours post-transfection (hpt) and dissociated in 0.05% trypsin followed by cell sorting (BD FACS Aria™ SORP) based on the GFP signal intensity. 50,000 GF:cells were obtained for RNA extraction (TaKaRa 9767), cDNA synthesis for (TaKaRa RR036A) cloning into plasmid (99139_U6.3 gRNA f+e) for genotyping. A specific

primer (cctataaaaataggcgtatcacg) was used for genotyping sequencing (Centre for PanorOmic Sciences, the University of Hong Kong).

RNA-seq

RNA-seq was performed on RNAs extracted from the sorted cells of transfected chick embryos. Approximately 50,000 GFP+ cells per treatment were collected for RNA extraction using RNAqueous-Micro Kit (Ambion) and genomic DNA was removed by TURBO DNase treatment for 30 min. RNA quality was assayed in an Agilent 2100 Bioanalyzer and samples with an RNA integrity number (RIN) ≥8.0 and 28S/18S ≥ 1.0 were further processed. Samples were sent to the Beijing Genomics Institute (BGI) for RNA-sequencing. High-quality RNA (~50 ng) was used for RNA amplification and cDNA synthesis. The cDNA with adapter was further amplified to make a library of single stranded circular DNA, which were used to generate DNA nanoballs (DNBs) by rolling circle replication for the enhancement of fluorescence signals during the sequencing process. The DNBs were loaded into the patterned nanoarrays for 100-bp pair-end sequencing in a BGISEQ-500 platform. Biological replicates were used for each condition (Cas9 + *PHF5A* or *SF3B1* or *DLC1 gRNA*). Analysis was performed using program Intron Retention Finder (IRFinder) and R Studio.

***In situ* hybridization**

In situ hybridization was performed on HH10 chick embryos with anti-sense DIG-riboprobes for *PHF5A*, *SF3B1*, *DLC1*, *SOX9*, *SNAI2, FOXD3, WNT1* and *BMP4* generated from pBluescript-II KS vector and purified using G-50 column (GE Healthcare). Transfected embryos were fixed in 4% PFA overnight at 4 ℃, washed (PBS, 0.1% Tween-20) and dehydrated through 25%, 50%, 75% methanol/PBS, 0.1% Tween-20 then absolute methanol. Embryos can be stored at -20 ℃ at this

point or processed for the rest of the hybridization procedure which took four days. Day 1, embryos were rehydrated through 75%, 50%, 25%, 0 methanol/PBS, 0.1% Tween-20, then bleached in 6% H_2O_2/PBS, 0.1% Tween-20, incubated in 10 μg/mL proteinase K solution (Invitrogen™, 25530049), post-fixed, pre-hybridized for 1 h and hybridized in solution containing anti-sense probe overnight at 70^0C. Day 2, embryos were extensively washed to remove unbound probe, blocked in 10% sheep serum (Sigma, S3772) for 60-90 min at room temperature then incubated in anti-DIG-AP (Roche, 11093274910) diluted in 1% sheep serum overnight at 4 ℃. Day 3, embryos were extensively washed in 1 × TBST 5 times one hour each and incubated in TBST overnight at room temperature. Day 4, embryos were subjected to color development using NBT/BCIP detection kit (1:50, Roche). The duration of color development varied depending on the expression level for each gene. Embryos were fixed (4% PFA overnight at 4 ℃) and embedded (Tissue freezing medium, Leica) for cryosectioning.

Whole mount immunofluorescence

Whole mount immunofluorescence (IF) was conducted in transfected embryos which were fixed in 4% PFA overnight at 4 ℃ and then blocked in blocking buffer (PBS+1% Triton, 10% FBS, 0.02% NaN_3) for an hour. Embryos were then incubated with primary antibodies (1: 1000 anti-rabbit GFP, Invitrogen and 1: 400 anti-mouse HNK-1, Developmental studies hybridoma bank (DSHB) blocking buffer for 2 days 4 ℃ with gentle rocking, washed 3 times 30 min each in washing buffer (PBS+1% Triton) followed by 2 days incubation with secondary antibodies (Alexa Fluor™ 488, Jackson Immuno Research, and Cy™3 AffiniPure donkey anti-mouse IgM) in blocking buffer at 4^0C overnight. The embryos were washed 3 times 30 min each in washing buffer before imaging.

Cryosectioning

The whole mount immunostained embryos were embedded (Tissue freezing medium, Leica) and cryosectioned at 12 μm (Thermo Fisher Scientific, CryoStar NX50) for immunofluorescence imaging or transfected embryos freshly dissected, fixed (4% PFA at 4 ℃ for 2 h), dehydrated (30% sucrose at 4 ℃ overnight) and embedded with tissue freezing medium in silicone molds and snap freezing at -80 °C for cryosectioning.

Immunofluorescence

Transverse sections were washed in (PBS+0.1% Triton) to remove the OCT (Tissue freezing medium, Leica) and then blocked in blocking buffer (1% BSA in 1 × PBS 0.1% Triton) for 20 min before incubating with primary antibodies (anti-sheep GFP, Bio Rad, anti-rabbit RFP, Rockland, anti-mouse HA tag, Invitrogen, anti-mouse V5 tag, Invitrogen, anti-rabbit SOX9, Merck Millipore, anti-goat SOX2, R&D, anti-rabbit Caspase-3, Cell signaling technology, anti-mouse PAX7, Developmental studies hybridoma bank) at 4 ℃ overnight, washed (1 × PBS 0.1% Triton) three times and incubated with secondary antibodies (Alexa Fluor™ 488, 594, 647) at room temperature 1-2 h. Stained with DAPI (1:1000 in 1 × PBS) at room temperature for 5 min before mounting (Fluorescence mounting medium, Dako) the slides with cover slips. All incubations were conducted in a humidified chamber.

Imaging

The images of whole mount IF were taken by Leica MZ10F microscopy. Imaging of *in situ* hybridization and section IF were performed using Zeiss Axiophot microscopy and Zeiss LSM780 confocal microscopy, respectively.

Hybridization chain reaction (HCR)

Electroporated and/or PB-treated embryos were collected at designated time points and placed in a petri dish containing Ringer's solution. They were then rinsed once before fixation in 4% PFA, at 4 ℃ for 14 h. Fixed embryos were treated with pre-warmed (37 ℃) 10 μg/mL proteinase K solution for 10 min, followed by post-fixation with 4% PFA at room temperature for 20 min. The embryos were then washed in PBST, 50% PBST / 50% 5× SSCT, 5× SSCT subsequently. First, the detection procedure involved the following steps: (1) Transfer 1-4 embryos to a 2 mL tube for each sample. (2) Pre-hybridize the embryos in 500 μL of probe hybridization buffer for 30 min at 37 ◦C. (3) Prepare the probe solution by adding 2 pmol of each probe set (e.g. 2 μL of 1 μM stock) to 500 μL of probe hybridization buffer at 37 ◦C. (4) Remove the pre-hybridization solution and add the probe solution. (5) Incubate the embryos overnight (>12 h) at 37 ◦C. (6) Remove excess probes by washing embryos 4 × 15 min with 1 mL of probe wash buffer at 37 ◦C. (7) Wash the samples 2 × 5 min with 5× SSCT at room temperature. Second, the amplification procedure involved the following steps: (1) Pre-amplify the embryos with 500 μL of amplification buffer for 5 min at room temperature. (2) Prepare 30 pmol of hairpin h1 and 30 pmol of hairpin h2 separately by snap cooling 10 μL of 3 μM stock (heat at 95 ◦C for 90 seconds and cool to room temperature in a dark drawer for 30 min). (3) Prepare the hairpin solution by adding the snap-cooled h1 hairpins and snap-cooled h2 hairpins to 500 μL of amplification buffer at room temperature. (4) Remove the pre-amplification solution and add the hairpin solution. (5) Incubate the embryos overnight (>12 h) in the dark at room temperature. (6) Wash off excess hairpins with 1 mL of 5× SSCT at room temperature: (a) 2 × 5 min (b) 2 × 30 min (c) 1 × 5 min (7) Samples can be stored at 4 ◦C protected from light before embedding, cryosectioning and imaging. List of HCR probe sequences

for *DLC1*, *PHF5A*, *SF3B1*, *SOX9*, *SNAI2*, *SNAI2 intron 1*, *SNAI2 intron 3* are shown in Table S6-12 respectively.

Mass spectrometry

DLC1 antibody and IgG control were used to immunoprecipitate endogenous DLC1 and their associated proteins from lysates of chick embryos (30 embryos per sample). Coomassie blue staining (QC Colloidal Coomassie Stain, BioRad 1610803) visualized multiple distinct and unique bands of proteins immunoprecipitated by DLC1 antibody but not IgG control to confirm the specificity of pull-down. The samples were run through the stacking gel of SDS-PAGE until reaching the boundary of stacking and separating gel. The Coomassie blue-stained bands from the samples were excised from the gel and sent to the Centre for PanorOmic Sciences, Li Ka Shing Faculty of Medicine, the University of Hong Kong for mass spectrometry analysis to identify the partner factors of DLC1. The same approach was applied to identify PHF5A-associated proteins. Gene ontology analysis was conducted using mass spectrometry data and exported by Cytoscape 3.10.0.

Immunoprecipitation and RNA-immunoprecipitation (RIP)-qPCR

Wild-type chick embryos or electroporated chick embryos were dissociated in IP lysis buffer plus protease and phosphatase inhibitors (Invitrogen™ Halt™ Protease and Phosphatase inhibitor cocktail, 100x, 78442) or ribonuclease inhibitors (Invitrogen™ RNaseOUT™, 10777019) and 10% lysate from each treatment was reserved as input control and stored at -80^{0}C for further analysis. The rest of the lysates from each treatment were incubated with antibodies in tubes on a rotating wheel overnight at 4 ℃ to form the immune complex. 25 μL beads (Thermo Scientific 90409) were added into each treatment and incubated for 4 h on rocking at 4 ℃. The samples were then washed

and bead-immune complexes were collected with the assistance of a magnetic stand. Subsequently, the immunoprecipitated lysates from each sample together with 10% inputs were mixed with 1 × loading dye and boiled for 10 min at 95 ℃ to dissociate the immunocomplexes from the beads. The resulting samples were analyzed by Western blot or reverse transcription quantitative polymerase chain reaction (RT-qPCR) with primers shown in Table S2.

Western blot

Electroporated chick embryos were dissociated in RIPA buffer (0.1% SDS, 1% NP-40, 1% sodium deoxycholate, 150mM NaCl, 25mM Tris-HCl pH 7.6), lysed on ice for 40 min, vortex every 10 min then centrifuged for 15 min at 16000 g at 4 ℃ to collect supernatants. BCA (Thermo Scientific, 23228) approach followed by establishment of standard curve was applied to measure the concentrations of lysates. Samples can be stored at -80 ℃ for further analysis or immediate processing. To detect the expression levels of endogenous protein or protein-protein interaction, the protein lysates were run at different percentage of SDS-PAGE based on the molecular weight of protein of interest. The duration of transfer also varied based on the protein mass. The protein bands were visualized (Advansta, K-12045-D50. Carestream dental GBX, 661 0091) in films (Fujifilm, 47410 19274) following incubation of primary (anti-rabbit PHF5A, Proteintech, anti-mouse SF3B1, MBL, anti-rabbit DLC1, BD Biosciences, anti-rabbit cleaved caspase-3, Cell Signaling Technology, anti-mouse RNA Pol II, Cell Signaling Technology, anti-rabbit RNA Pol II Ser5, Cell Signaling Technology, anti-rabbit RNA Pol II Ser2, Cell Signaling Technology) and secondary (anti-mouse IgG HRP, anti-rabbit IgG HRP, Thermo Fisher Scientific) antibodies. Quantification of protein band intensity on Western blots was conducted by Adobe Photoshop 2021.

In vitro protein-RNA binding assay

The chick cDNA encoding *DLC1*, *PHF5A,* and *SF3B1* was cloned into the pET-30 plasmid. Each construct was then transformed into Rosetta® cells, which were cultured in LB for protein expression (at 15 ℃ for 16 h) with the addition of 0.5 mM IPTG (GoldBio, I2481C100). The proteins were sonicated, collected, and purified, and then incubated together with biotinylated introns of *SOX9* or *SNAI2* (IDT, sequences listed in Table 1) at 4 ℃ for14 h with mild rotation. The mixtures were further incubated, concentrated, and purified using streptavidin agarose (Millipore, 69203-3CN). Finally, Western blot analysis was performed using an anti-HIS antibody (Invitrogen, MA1-135) to detect the bound proteins.

Reverse transcription polymerase chain reaction, intron retention and statistical analysis

Semi-quantitative RT-PCRs (Vazyme, 2 × Rapid Taq Master Mix, P222-02) were performed in embryos with different gRNA treatments to analyze the levels of unspliced and spliced transcripts as well as exon skipping. Quantification of DNA band intensity was conducted by Adobe Photoshop 2021. RT-qPCRs (TaKaRa, TB Green™ Premix Ex Taq ™ II, RR820A) were performed with cDNAs produced from sorted cells (BD FACSAria SORP) to analyze the expression levels of NC specifier genes or with cDNAs generated from RNAs in intron retention analysis (Table S2). List of primers used for semi-quantitative RT-PCR, RT-qPCR and ChIP-qPCR are shown in Table S3, S4 and S5 respectively.

Data from at least three separate experiments were presented as mean ± SD. Significant differences were shown as *: $p < 0.05$, **: $p < 0.01$, ***: $p < 0.001$, ****: $p < 0.000$, One-way ANOVA (GraphPad Prism 9).

Data availability

All data supporting the conclusion of this study are present in the manuscript and/or the Supplementary Materials. All raw data from mass spectrometry and RNA sequencing are available in Dataset S1, Dataset S2, and Dataset S3, respectively.

Acknowledgments

We thank the members of M. Cheung's laboratory, R. Fässler, S.C. Kwon, T. Cheung, Z.J. Zhou, and B. Gao for their helpful discussions. We thank the members of M.E. Bronner's laboratory for advice on the generation of the CRISPR-Cas9/gRNA constructs and members of Ni Tao's laboratory for advice on in vitro protein binding assay. We also thank the technical staff of the Centre for PanorOmic Sciences for their advice on the confocal imaging and FACS analysis.

Funding

The work is supported by Hong Kong Research Grants Council General Research Fund (Project no. 17101622, 17102420) and Seed Fund for Basic Research, HKU (Project no. 202011159132, 201910159225) to M.C. Z.F.Z was supported by the postgraduate scholarship HKU and General Research Fund.

Author contributions

Conceptualization: Z.F.Z., J.A.I.J., and M.C. Investigation: Z.F.Z., S.S.G., Y.X.R. and M.N.H. Methodology: Z.F.Z., S.S.G., Y.X.R., K.K.W.W., R.S., M.P.L.C. and H.Y.T. Visualization: Z.F.Z. Funding acquisition: Z.F.Z., and M.C. Supervision: M.C. Writing (original draft): Z.F.Z., and M.C. Writing (review & editing): Z.F.Z., and M.C.

Competing interests

The authors declare that they have no competing interests.

References

1. Basch ML, Bronner-Fraser M, Garcia-Castro MI. Specification of the neural crest occurs during gastrulation and requires Pax7. *Nature* **441**, 218-222 (2006).

2. Liu JA, Cheung M. Neural crest stem cells and their potential therapeutic applications. *Dev Biol* **419**, 199-216 (2016).

3. Stuhlmiller TJ, Garcia-Castro MI. Current perspectives of the signaling pathways directing neural crest induction. *Cell Mol Life Sci* **69**, 3715-3737 (2012).

4. Monsoro-Burq AH, Wang E, Harland R. Msx1 and Pax3 cooperate to mediate FGF8 and WNT signals during Xenopus neural crest induction. *Dev Cell* **8**, 167-178 (2005).

5. Simoes-Costa M, Stone M, Bronner ME. Axud1 Integrates Wnt Signaling and Transcriptional Inputs to Drive Neural Crest Formation. *Dev Cell* **34**, 544-554 (2015).

6. Cheung M, Briscoe J. Neural crest development is regulated by the transcription factor Sox9. *Development* **130**, 5681-5693 (2003).

7. Cheung M, Chaboissier MC, Mynett A, Hirst E, Schedl A, Briscoe J. The transcriptional control of trunk neural crest induction, survival, and delamination. *Dev Cell* **8**, 179-192 (2005).

8. Beauchamp MC, Alam SS, Kumar S, Jerome-Majewska LA. Spliceosomopathies and neurocristopathies: Two sides of the same coin? *Dev Dyn* **249**, 924-945 (2020).

9. Kambach C, Walke S, Nagai K. Structure and assembly of the spliceosomal small nuclear ribonucleoprotein particles. *Curr Opin Struct Biol* **9**, 222-230 (1999).

10. Wahl MC, Will CL, Luhrmann R. The spliceosome: design principles of a dynamic RNP machine. *Cell* **136**, 701-718 (2009).

11. Lardelli RM, Thompson JX, Yates JR, 3rd, Stevens SW. Release of SF3 from the intron branchpoint activates the first step of pre-mRNA splicing. *RNA* **16**, 516-528 (2010).

12. Isono K, Abe K, Tomaru Y, Okazaki Y, Hayashizaki Y, Koseki H. Molecular cloning, genetic mapping, and expression of the mouse Sf3b1 (SAP155) gene for the U2 snRNP component of spliceosome. *Mamm Genome* **12**, 192-198 (2001).

13. Isono K, Mizutani-Koseki Y, Komori T, Schmidt-Zachmann MS, Koseki H. Mammalian polycomb-mediated repression of Hox genes requires the essential spliceosomal protein Sf3b1. *Genes Dev* **19**, 536-541 (2005).

14. Lim DA, Suarez-Farinas M, Naef F, Hacker CR, Menn B, Takebayashi H, Magnasco M, Patil N, Alvarez-Buylla A. In vivo transcriptional profile analysis reveals RNA splicing and chromatin remodeling as prominent processes for adult neurogenesis. *Mol Cell Neurosci* **31**, 131-148 (2006).

15. Wang C, Sashida G, Saraya A, Ishiga R, Koide S, Oshima M, Isono K, Koseki H, Iwama A. Depletion of Sf3b1 impairs proliferative capacity of hematopoietic stem cells but is not sufficient to induce myelodysplasia. *Blood* **123**, 3336-3343 (2014).

16. An M, Henion PD. The zebrafish sf3b1b460 mutant reveals differential requirements for the sf3b1 pre-mRNA processing gene during neural crest development. *Int J Dev Biol* **56**, 223-237 (2012).

17. Trappe R, Ahmed M, Glaser B, Vogel C, Tascou S, Burfeind P, Engel W. Identification and characterization of a novel murine multigene family containing a PHD-finger-like motif. *Biochem Biophys Res Commun* **293**, 816-826 (2002).

18. Yan C, Wan R, Bai R, Huang G, Shi Y. Structure of a yeast activated spliceosome at 3.5 A resolution. *Science* **353**, 904-911 (2016).

19. Rzymski T, Grzmil P, Meinhardt A, Wolf S, Burfeind P. PHF5A represents a bridge protein between splicing proteins and ATP-dependent helicases and is differentially expressed during mouse spermatogenesis. *Cytogenet Genome Res* **121**, 232-244 (2008).

20. Cordin O, Beggs JD. RNA helicases in splicing. *RNA Biol* **10**, 83-95 (2013).

21. Finci LI, Zhang X, Huang X, Zhou Q, Tsai J, Teng T, Agrawal A, Chan B, Irwin S, Karr C, Cook A, Zhu P, Reynolds D, Smith PG, Fekkes P, Buonamici S, Larsen NA. The cryo-EM structure of the SF3b spliceosome complex bound to a splicing modulator reveals a pre-mRNA substrate competitive mechanism of action. *Genes Dev* **32**, 309-320 (2018).

22. Teng T, Tsai JH, Puyang X, Seiler M, Peng S, Prajapati S, Aird D, Buonamici S, Caleb B, Chan B, Corson L, Feala J, Fekkes P, Gerard B, Karr C, Korpal M, Liu X, J TL, Mizui Y, Palacino J, Park E, Smith PG, Subramanian V, Wu ZJ, Zou J, Yu L, Chicas A, Warmuth M, Larsen N, Zhu P. Splicing modulators act at the branch point adenosine binding pocket defined by the PHF5A-SF3b complex. *Nat Commun* **8**, 15522 (2017).

23. Cretu C, Gee P, Liu X, Agrawal A, Nguyen TV, Ghosh AK, Cook A, Jurica M, Larsen NA, Pena V. Structural basis of intron selection by U2 snRNP in the presence of covalent inhibitors. *Nat Commun* **12**, 4491 (2021).

24. Butt H, Bazin J, Alshareef S, Eid A, Benhamed M, Reddy ASN, Crespi M, Mahfouz MM. Overlapping roles of spliceosomal components SF3B1 and PHF5A in rice splicing regulation. *Commun Biol* **4**, 529 (2021).

25. Vigevani L, Gohr A, Webb T, Irimia M, Valcarcel J. Molecular basis of differential 3' splice site sensitivity to anti-tumor drugs targeting U2 snRNP. *Nat Commun* **8**, 2100 (2017).

26. Oltra E, Pfeifer I, Werner R. Ini, a small nuclear protein that enhances the response of the connexin43 gene to estrogen. *Endocrinology* **144**, 3148-3158 (2003).

27. Karmakar S, Rauth S, Nallasamy P, Perumal N, Nimmakayala RK, Leon F, Gupta R, Barkeer S, Venkata RC, Raman V, Rachagani S, Ponnusamy MP, Batra SK. RNA Polymerase II-Associated Factor 1 Regulates Stem Cell Features of Pancreatic Cancer

Cells, Independently of the PAF1 Complex, via Interactions With PHF5A and DDX3. *Gastroenterology* **159**, 1898-1915 e1896 (2020).

28. Strikoudis A, Lazaris C, Trimarchi T, Galvao Neto AL, Yang Y, Ntziachristos P, Rothbart S, Buckley S, Dolgalev I, Stadtfeld M, Strahl BD, Dynlacht BD, Tsirigos A, Aifantis I. Regulation of transcriptional elongation in pluripotency and cell differentiation by the PHD-finger protein Phf5a. *Nat Cell Biol* **18**, 1127-1138 (2016).

29. Liu JA, Rao Y, Cheung MPL, Hui MN, Wu MH, Chan LK, Ng IO, Niu B, Cheah KSE, Sharma R, Hodgson L, Cheung M. Asymmetric localization of DLC1 defines avian trunk neural crest polarity for directional delamination and migration. *Nat Commun* **8**, 1185 (2017).

30. Hamburger V, Hamilton HL. A series of normal stages in the development of the chick embryo. 1951. *Dev Dyn* **195**, 231-272 (1992).

31. Shilatifard A, Conaway RC, Conaway JW. The RNA polymerase II elongation complex. *Annu Rev Biochem* **72**, 693-715 (2003).

32. Golas MM, Sander B, Will CL, Luhrmann R, Stark H. Molecular architecture of the multiprotein splicing factor SF3b. *Science* **300**, 980-984 (2003).

33. Sciarrillo R, Wojtuszkiewicz A, El Hassouni B, Funel N, Gandellini P, Lagerweij T, Buonamici S, Blijlevens M, Zeeuw van der Laan EA, Zaffaroni N, Deraco M, Kusamura S, Wurdinger T, Peters GJ, Molthoff CFM, Jansen G, Kaspers GJL, Cloos J, Giovannetti E. Splicing modulation as novel therapeutic strategy against diffuse malignant peritoneal mesothelioma. *EBioMedicine* **39**, 215-225 (2019).

34. Marasco LE, Kornblihtt AR. The physiology of alternative splicing. *Nat Rev Mol Cell Biol*, (2022).

35. Zheng YZ, Xue MZ, Shen HJ, Li XG, Ma D, Gong Y, Liu YR, Qiao F, Xie HY, Lian B, Sun WL, Zhao HY, Yao L, Zuo WJ, Li DQ, Wang P, Hu X, Shao ZM. PHF5A Epigenetically Inhibits Apoptosis to Promote Breast Cancer Progression. *Cancer Res* **78**, 3190-3206 (2018).

36. Cretu C, Agrawal AA, Cook A, Will CL, Fekkes P, Smith PG, Luhrmann R, Larsen N, Buonamici S, Pena V. Structural Basis of Splicing Modulation by Antitumor Macrolide Compounds. *Mol Cell* **70**, 265-273 e268 (2018).

37. Wong JJ, Au AY, Ritchie W, Rasko JE. Intron retention in mRNA: No longer nonsense: Known and putative roles of intron retention in normal and disease biology. *Bioessays* **38**, 41-49 (2016).

38. Yang Y, Li M, Zhou X, Wang W, Shao Y, Yao J, Wang X. PHF5A Contributes to the Maintenance of the Cancer Stem-like Phenotype in Non-Small Cell Lung Cancer by Regulating Histone Deacetylase 8. *Ann Clin Lab Sci* **52**, 439-451 (2022).

39. Yang X, Hu F, Liu JA, Yu S, Cheung MPL, Liu X, Ng IO, Guan XY, Wong KKW, Sharma R, Lung HL, Jiao Y, Lee LTO, Cheung M. Nuclear DLC1 exerts oncogenic function through association with FOXK1 for cooperative activation of MMP9 expression in melanoma. *Oncogene* **39**, 4061-4076 (2020).

40. Berube-Simard FA, Pilon N. Molecular dissection of CHARGE syndrome highlights the vulnerability of neural crest cells to problems with alternative splicing and other transcription-related processes. *Transcription* **10**, 21-28 (2019).

41. Soldatov R, Kaucka M, Kastriti ME, Petersen J, Chontorotzea T, Englmaier L, Akkuratova N, Yang Y, Haring M, Dyachuk V, Bock C, Farlik M, Piacentino ML, Boismoreau F, Hilscher MM, Yokota C, Qian X, Nilsson M, Bronner ME, Croci L, Hsiao WY, Guertin DA, Brunet JF, Consalez GG, Ernfors P, Fried K, Kharchenko PV, Adameyko I. Spatiotemporal structure of cell fate decisions in murine neural crest. *Science* **364**, (2019).

42. Park BY, Tachi-Duprat M, Ihewulezi C, Devotta A, Saint-Jeannet JP. The Core Splicing Factors EFTUD2, SNRPB and TXNL4A Are Essential for Neural Crest and Craniofacial Development. *J Dev Biol* **10**, (2022).

43. Devotta A, Juraver-Geslin H, Gonzalez JA, Hong CS, Saint-Jeannet JP. Sf3b4-depleted Xenopus embryos: A model to study the pathogenesis of craniofacial defects in Nager syndrome. *Dev Biol* **415**, 371-382 (2016).

44. Liu JA, Tai A, Hong J, Cheung MPL, Sham MH, Cheah KSE, Cheung CW, Cheung M. Fbxo9 functions downstream of Sox10 to determine neuron-glial fate choice in the dorsal root ganglia through Neurog2 destabilization. *Proc Natl Acad Sci U S A* **117**, 4199-4210 (2020).

Figure Legends

Figure 1. DLC1 is required for NC specification through the regulation of *SOX9* and *SNAI2* pre-mRNA splicing.

a Hybridization chain reaction (HCR) revealed the co-localization of *DLC1*, *SOX9,* and *SNAI2* mRNA in premigratory NCCs. **b** Schematic diagram of gRNA 1 and gRNA 2 oligos targeting different regions of *DLC1 exon 9*. **c** Experimental workflow. **d** Western blot showing loss of DLC1 expression in both gRNA treatment groups compared to control gRNA (Ctrl gRNA). **e** Reduced expression of *SOX9*, *SNAI2,* and *FOXD3* in dorsal neural tubes transfected with *DLC1 gRNA* shown by in situ hybridization (ISH) (blue arrowheads). Black arrows indicate unaltered and restored expression of *SOX9*, *SNAI2* and *FOXD3* in Ctrl gRNA and rescue treatments, respectively. Scale bar, 50 μm (*n*=3). **f to h** RT-qPCR demonstrating reduced expression levels of *SOX9*, *SNAI2* and *FOXD3* in *DLC1*-depleted cells compared to Ctrl gRNA (n=5). **i** Immunofluorescence (IF) illustrating nuclear localization of ectopic V5-DLC1 (open arrowheads) in the dorsal neural tube. **j** Electroporation of *DLC1 gRNA1* leading to reduced SOX9 expression (white open arrowheads) and upregulated SOX2 expression (white solid arrowheads) in the dorsal neural tube. Dotted lines outline the neural tube. Scale bar, 50 μm (*n*=3 per group). **k** Whole mount IF and the transverse sections reveal reduced expression of HNK-1 (white open arrowheads) in *DLC1 gRNA 1* transfected side. White dotted lines in the whole mount IF indicate the axial level of transverse sections. Scale bar, 100 μm (n=3). **l** Western blot showing unaltered expression of RNA Pol II-pSer5 and -pSer2 in embryos treated with *DLC1 gRNA 1* and *gRNA 2* compared to *Ctrl gRNA* (n=10 per group). Intron retention-qPCR (IR-qPCR) analysis indicated increased levels of *SOX9 introns 1/2* (**m**) and *SNAI2 introns 1/3* (**o**) in embryos treated with *DLC1 gRNA1* compared to *Ctrl gRNA* (n=5). Schematic diagram illustrating intron-retained *SOX9* (**n**) and *SNAI2* (**p**) pre-mRNA in *DLC1*-depleted cells. Arrows indicate primer pairs flanking the branch point adenosine (A) in each intron for qPCR analysis. **q** HCR showing the detection of retained intron1/2 of *SOX9* and introns 1/3 of *SNAI2* in dorsal neural tubes transfected with *DLC1 gRNA1*, while no signal was detected in *Ctrl gRNA* (n=3). Dotted lines outline the transverse neural tubes where the "+" indicates the transfected side. Scale bar, 50 μm. Mean ± SD. **: $p < 0.01$, ***: $p < 0.001$.

Figure 2. PHF5A, an interacting factor of DLC1, plays a crucial role in NC specification by regulating the splicing of *SOX9* and *SNAI2* pre-mRNA.

a Interactome of DLC1-associated splicing factors. Proteins of interest, PHF5A and SF3B1, are color-coded in brown. Immunoprecipitation (IP) validated the association of endogenous DLC1 with PHF5A and SF3B1. **b** Interactome of PHF5A showing splicing factors in the SF3B complex (green color). IP confirmed the association of endogenous SF3B1 with PHF5A. **c** Schematic diagram of gRNA 1 and gRNA 2 oligos targeting exon 3 and exon 4 of *PHF5A*. Western blot showing abolishment of PHF5A expression in embryos treated with *PHF5A gRNA* compared to embryos treated with *Ctrl gRNA* (n=10). IF and ISH show reduced expression (white open arrowheads) of *SOX9* (**d**), *SNAI2* (**f**), and *FOXD3* (**h**) in *PHF5A*-ablated cells compared to *Ctrl gRNA*. **e**, **g** and **i** qRT-PCR confirmed the reduction of these genes. The expression of NC specifier genes was restored by pCIG-HA-PHF5A overexpression. Black arrows indicate unaltered expression of NC specifier genes in *Ctrl gRNA* embryos and restoration of NC specifier genes expression in the rescue groups. Scale bar, 50 μm (*n*=3 per group). **j** SOX9 expression (white open arrowheads) was reduced in *PHF5A*-depleted NCCs where SOX2 expression was upregulated (white solid arrowheads). Dotted lines outline the neural tube. Scale bar, 50 μm (*n*=3 per group). **k** HNK-1 expression was reduced (white open arrowheads) in the *PHF5A gRNA*-transfected side compared to the untransfected side and embryo treated with *Ctrl gRNA*. l Expression levels of RNA PolII-pSer5 and -pSer2 remained unaltered in *PHF5A KO* embryos compared to *Ctrl gRNA* (n=10). IR-qPCR analysis showed increased levels of *SOX9 introns 1/2* (**m**) and *SNAI2 introns 1/3* (**o**) in embryos treated with *PHF5A gRNA1* compared to *Ctrl gRNA*-treated embryos (n=5). Schematic diagram showing intron-retained *SOX9* and *SNAI2* pre-mRNA in *PHF5A*-ablated cells. Arrows indicate primer pairs for the detection of retained introns of *SOX9* (**n**) and *SNAI2* (**p**). **q** HCR showing detection of retained introns of *SOX9* and *SNAI2* in embryos transfected with *PHF5A gRNA*. Dotted lines outline the transverse neural tubes where the "+" indicates the transfected side. Scale bar: 50 μm. Mean ± SD. **: $p < 0.01$, ***: $p < 0.001$.

Figure 3. Transcriptomic profiling reveals increased intron retention of NC specifier genes in embryos lacking DLC1, PHF5A, or SF3B1 in the neural tubes.

Elevated intron expression levels of *SOX9* (**a**, **b**), *SNAI2* (**c**, **d**), *ID1* (**e**), *TWIST1* (**f**), and *MYC* (**g**) were detected in the absence of *DLC1*, *PHF5A*, or *SF3B1* compared to *Ctrl gRNA*.

Intron levels of *BMP4* (h), *WNT1* (**i**, **j**), *PAX7* (**k**, **l**, **m**), and *MYB* (**n**) were unaltered in embryos lacking DLC1, PHF5A, or SF3B1 in the neural tubes.

Figure 4. DLC1 is required for the binding of PHF5A and SF3B1 to the introns of NC specifier genes.

a, b Schematic diagram shows primer pairs flanking the BPA of *SOX9* (**a**) and *SNAI2* (**b**) introns for RNA-immunoprecipitation qPCR (RIP-qPCR). **c** to **h** Graphs show the binding capacity of endogenous PHF5A (**c, f**), SF3B1 (**d, g**), and DLC1 (**e, h**) to the BPA of *SOX9 introns 1* and *2* as well as *SNAI2 introns 1* and *3* (n=30 per group). (i) IP shows that SF3B1 remained associated with PHF5A in the absence of DLC1. **j** to **m** RIP-qPCR analysis reveals reduced binding capacity of PHF5A-SF3B1 splicing complex to *introns 1* and *2* of *SOX9,* as well as *introns 1* and *3* of *SNAI2* in embryos treated with *DLC1 gRNA1* compared to *Ctrl gRNA* (*n*=30 per group). Mean ± SD. *: $p < 0.05$, **: $p < 0.01$, ***: $p < 0.001$, ****: $p < 0.0001$

Figure 5. Splicing modulator PB specifically reduces the expression levels of NC specifier genes.

a Experimental workflow. **b** Reduced expression of *SOX9*, *SNAI2,* and *FOXD3* (open arrowheads) in NCCs of embryos treated with PB, whereas expression of these genes in NCCs (black arrows) and somites (So) remained unaltered in embryos treated with PBS (n=9 per treatment). **c** PB treatment did not alter the pattern of PAX7 expression (indicated by white arrows) and did not lead to apoptosis, as evidenced by the absence of Caspase-3+ cells. **d** PB treatment did not affect the expression levels of PHF5A, SF3B1, DLC1, and RNA Pol II, nor induce Caspase 3 expression compared to PBS Ctrl. **e** IP analysis revealed that endogenous SF3B1 remained associated with PHF5A and DLC1 in the presence of PB. **f** and **h** qPCR data demonstrated increased levels of *SOX9 intron 2* (**f**) and *SNAI2 intron 3* (**h**) in the PB treatment groups compared to the PBS Ctrl. No retention of *SOX9 intron 1* and *SNAI2 intron 3* was detected in the PB treatment group (n=5 per treatment). **g** and **i** Schematic diagrams illustrate the presence of *intron 2*-retained *SOX9* pre-mRNA (**g**) and *intron 1*-retained *SNAI2* (**i**) pre-mRNA after PB treatment. **j** The HCR analysis revealed the expression of *SOX9 intron 2* and *SNAI2 intron 1* in NCCs of embryos treated with PB, as compared to the PBS Ctrl. **k**-**n** 6 sections per treatment were used for the quantification of fluorescence intensities. **o** - **r** PB treatment reduced the binding of PHF5A and SF3B1 on both

SOX9 intron 2 (**o**, **q**) and *SNAI2 intron 1* (**p**, **r**) compared to PBS Ctrl. Scale bar: 50 μm. NT, neural tube. Mean ± SD. ***: $p < 0.001$, ****: $p < 0.0001$, ns: no significant difference.

Figure 6. DLC1 determines the increased vulnerability of trunk NCCs to PB treatment.

a Experimental workflow. **b** Ectopic DLC1 expression in somites reduced expression of SOX9 (**b**, **c**) and SNAI2 (**d**, **e**) in a cell-autonomous manner (open arrowheads) in the PB treatment group. Open arrowheads indicate loss of SOX9 and SNAI2 expression in pre-migratory NCCs. There was no alteration of SOX9 (**b**, **c**) and SNAI2 (**d**, **e**) expression in DLC1-overexpressing somites and in NCCs (black and white arrows) in the PBS treatment group. Scale bar, 50 μm. Yellow dotted boxes outline the magnified view in the rightmost column of each panel. **f** IP shows the association of ectopic DLC1 with endogenous PHF5A and SF3B1 in somites of embryos treated with PBS Ctrl and PB. **g** and **i** Electroporation of DLC1 in somites resulted in increased levels of *SOX9 intron 2* and *SNAI2 intron 1* in the presence of PB compared to PBS Ctrl (n=5 per group). **h** and **j** Schematic diagrams depict the presence of *intron 2*-retained *SOX9* pre-mRNA (**h**) and *intron 1*-retained *SNAI2* pre-mRNA (**j**) in DLC1 overexpressing somites of embryos treated with PB. **k** The HCR analysis revealed the expression of *SOX9 intron 2* and *SNAI2 intron 1* in DLC1-overexpressing somites (So) of embryos treated with PB, as compared to the PBS Ctrl (n=5). **l-o** 20 sections per treatment were used for the quantification of fluorescence intensities. NT, neural tube. Scale bar: 50 μm. Mean ± SD. ***: $p < 0.001$, ****: $p < 0.0001$, ns: no significant difference.

Figure 7. The binding of the DLC1-SF3B1-PHF5A complex to shorter introns of NC specifier genes renders them more susceptible to splicing perturbation by PB

a, b Overexpression of DLC1 in somites of embryos treated with PB resulted in reduced binding capacity of PHF5A to *SOX9 intron 2* (**a**) and *SNAI2 intron 1* (**b**) compared to PBS Ctrl. **c**, **d** Overexpression of DLC1 in somites of embryos treated with PB led to a reduction in the binding capacity of SF3B1 to *SOX9 intron 2* (**c**) and *SNAI2 intron 1* (**d**) compared to PBS Ctrl. **e** In vitro translated SF3B1, DLC1, and PHF5A proteins, each fused with an HIS-tagged, failed to bind to the biotinylated *SOX9 intron 2* and *SNAI2 intron 1* in the presence of PB. However, PB did not alter the ability of these proteins to bind to the biotinylated *SOX9 intron 1* and *SNAI2 intron 3*. **f** Schematic diagram depicts the regulation of *SOX9* and *SNAI2* pre-mRNA splicing in prospective NCCs by the ubiquitously expressed SF3B1-PHF5A splicing factors, in association with NC-

specific DLC1. The DLC1-SF3B1-PHF5A splicing complex plays a crucial role in determining NCC fate and makes them more susceptible to the splicing modulator PB. This susceptibility is due to competitive inhibition of BPA recognition by the complex, which occurs in both *SOX9 intron 2* and *SNAI2 intron 1* due to their shorter length and weak Py tract, resulting in intron retention and loss of NC progenitors. Mean ± SD. **: $p < 0.01$; ***: $p < 0.001$, ns: no significant difference.

Figures

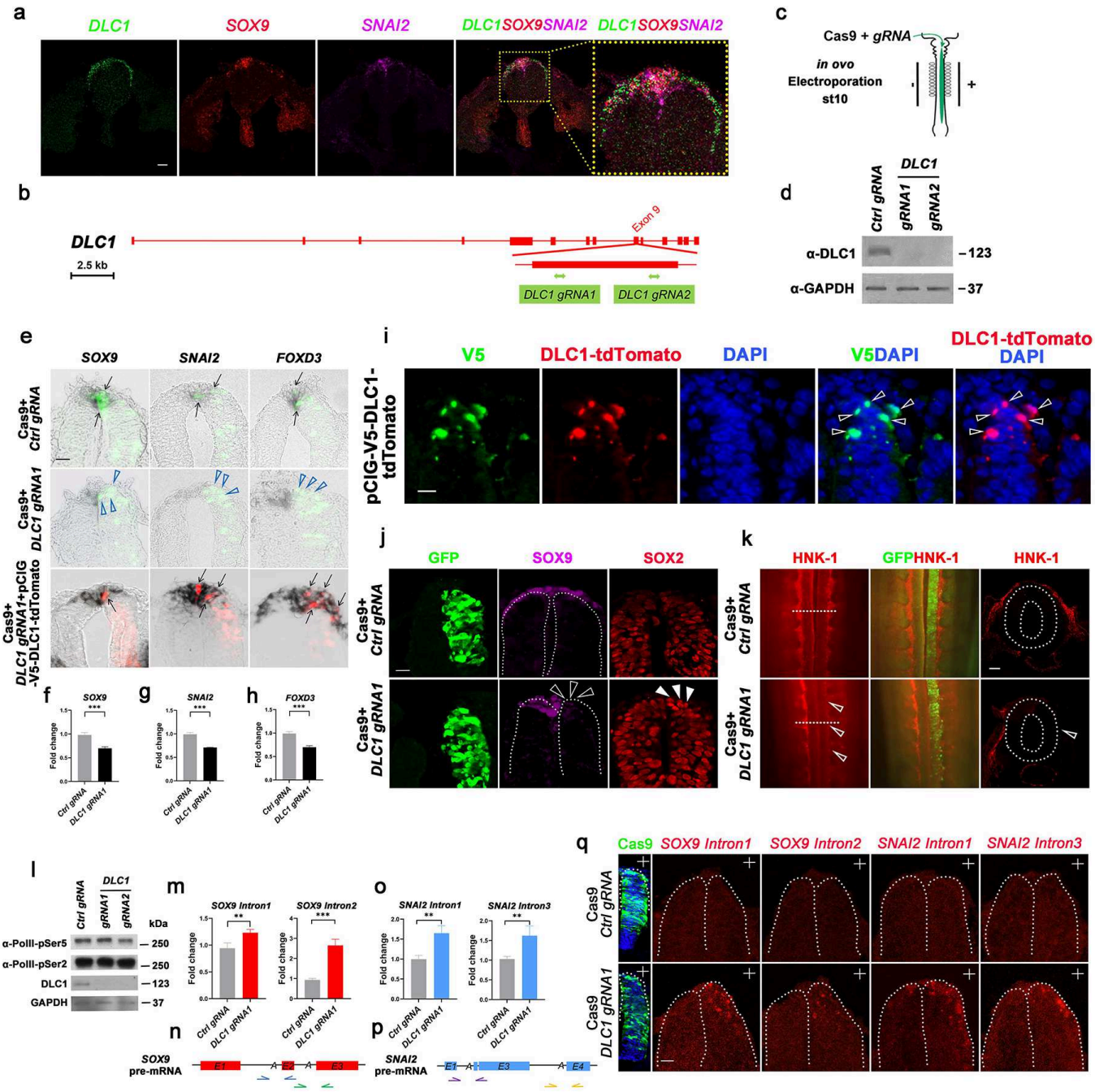


Figure 1

DLC1 is required for NC specification through the regulation of SOX9 and SNAI2 pre-mRNA splicing. a Hybridization chain reaction (HCR) revealed the co-localization of DLC1, SOX9, and SNAI2 mRNA in premigratory NCCs. b Schematic diagram of gRNA 1 and gRNA 2 oligos targeting different regions of

DLC1 exon 9. c Experimental workflow. d Western blot showing loss of DLC1 expression in both gRNA treatment groups compared to control gRNA (Ctrl gRNA). e Reduced expression of SOX9, SNAI2, and FOXD3 in dorsal neural tubes transfected with DLC1 gRNA shown by in situ hybridization (ISH) (blue arrowheads). Black arrows indicate unaltered and restored expression of SOX9, SNAI2 and FOXD3 in Ctrl gRNA and rescue treatments, respectively. Scale bar, 50 μm (n=3). f to h RT-qPCR demonstrating reduced expression levels of SOX9, SNAI2 and FOXD3 in DLC1-depleted cells compared to Ctrl gRNA (n=5). i Immunofluorescence (IF) illustrating nuclear localization of ectopic V5-DLC1 (open arrowheads) in the dorsal neural tube. j Electroporation of DLC1 gRNA1 leading to reduced SOX9 expression (white open arrowheads) and upregulated SOX2 expression (white solid arrowheads) in the dorsal neural tube. Dotted lines outline the neural tube. Scale bar, 50 μm (n=3 per group). k Whole mount IF and the transverse sections reveal reduced expression of HNK-1 (white open arrowheads) in DLC1 gRNA 1 transfected side. White dotted lines in the whole mount IF indicate the axial level of transverse sections. Scale bar, 100 μm (n=3). l Western blot showing unaltered expression of RNA Pol Ⅱ- pSer5 and -pSer2 in embryos treated with DLC1 gRNA 1 and gRNA 2 compared to Ctrl gRNA (n=10 per group). Intron retention-qPCR (IR-qPCR) analysis indicated increased levels of SOX9 introns 1/2 (m) and SNAI2 introns 1/3 (o) in embryos treated with DLC1 gRNA1 compared to Ctrl gRNA (n=5). Schematic diagram illustrating intron-retained SOX9 (n) and SNAI2 (p) pre-mRNA in DLC1-depleted cells. Arrows indicate primer pairs flanking the branch point adenosine (A) in each intron for qPCR analysis. q HCR showing the detection of retained intron1/2 of SOX9 and introns 1/3 of SNAI2 in dorsal neural tubes transfected with DLC1 gRNA1, while no signal was detected in Ctrl gRNA (n=3). Dotted lines outline the transverse neural tubes where the “+” indicates the transfected side. Scale bar, 50 μm. Mean ± SD. **: $p < 0.01$, ***: $p < 0.001$.

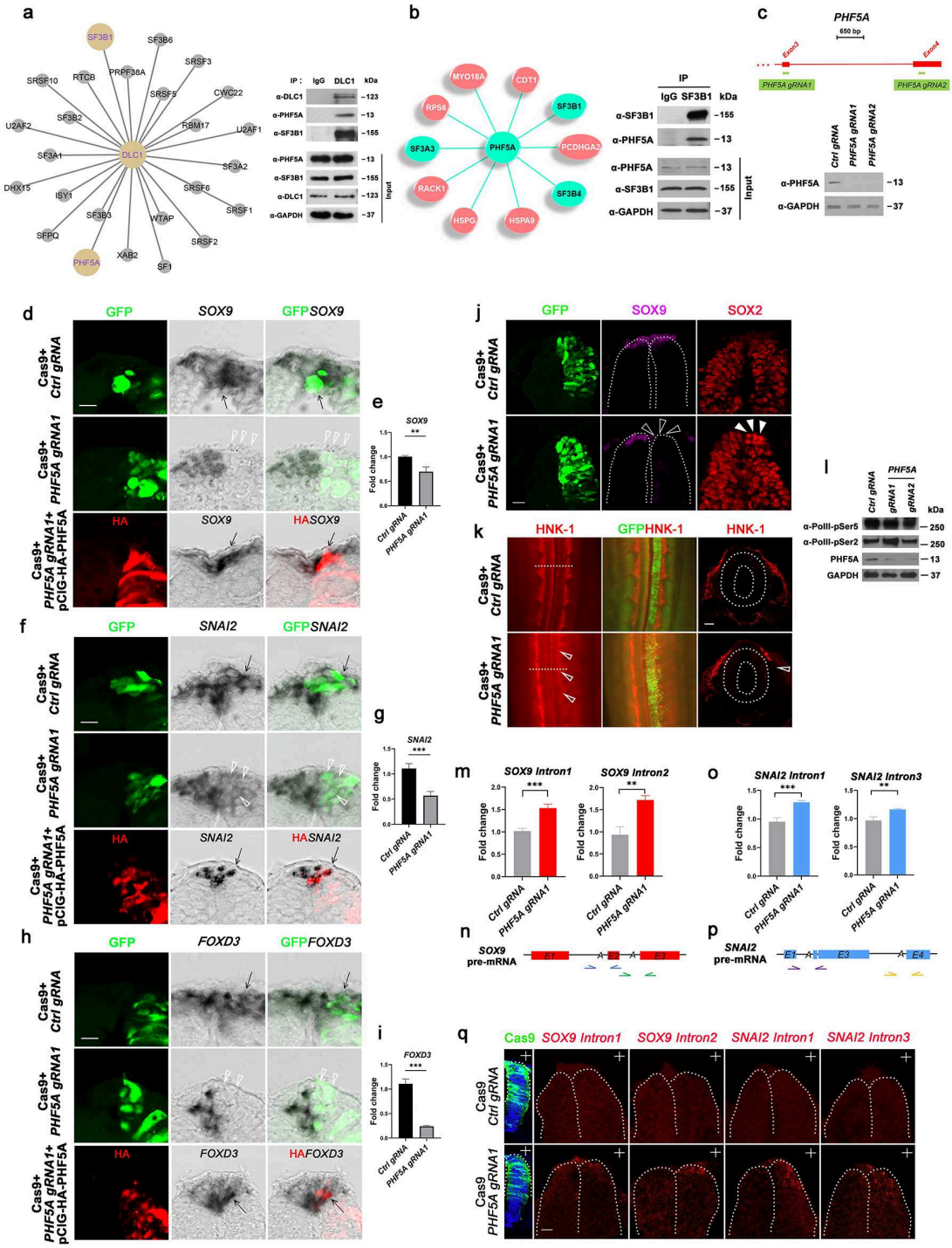


Figure 2

PHF5A, an interacting factor of DLC1, plays a crucial role 903 in NC specification by regulating the splicing of SOX9 and SNAI2 pre-mRNA. a Interactome of DLC1-associated splicing factors. Proteins of interest, PHF5A and SF3B1, are color-coded in brown. Immunoprecipitation (IP) validated the association of endogenous DLC1 with PHF5A and SF3B1. b Interactome of PHF5A showing splicing factors in the SF3B complex (green color). IP confirmed the association of endogenous SF3B1 with PHF5A. c

Schematic diagram of gRNA 1 and gRNA 2 oligos targeting exon 3 and exon 4 of PHF5A. Western blot showing abolishment of PHF5A expression in embryos treated with PHF5A gRNA compared to embryos treated with Ctrl gRNA (n=10). IF and ISH show reduced expression (white open arrowheads) of SOX9 (d), SNAI2 (f), and FOXD3 (h) in PHF5A-ablated cells compared to Ctrl gRNA. e, g and i qRT-PCR confirmed the reduction of these genes. The expression of NC specifier genes was restored by pCIG-HA-PHF5A overexpression. Black arrows indicate unaltered expression of NC specifier genes in Ctrl gRNA embryos and restoration of NC specifier genes expression in the rescue groups. Scale bar, 50 μm (n=3 per group). j SOX9 expression (white open arrowheads) was reduced in PHF5A-depleted NCCs where SOX2 expression was upregulated (white solid arrowheads). Dotted lines outline the neural tube. Scale bar, 50 μm (n=3 per group). k HNK-1 expression was reduced (white open arrowheads) in the PHF5A gRNA-transfected side compared to the untransfected side and embryo treated with Ctrl gRNA. l Expression levels of RNA Pol□-pSer5 and -pSer2 remained unaltered in PHF5A KO embryos compared to Ctrl gRNA (n=10). IR-qPCR analysis showed increased levels of SOX9 introns 1/2 (m) and SNAI2 introns 1/3 (o) in embryos treated with PHF5A gRNA1 compared to Ctrl gRNA-treated embryos (n=5). Schematic diagram showing intron-retained SOX9 and SNAI2 pre-mRNA in PHF5A-ablated cells. Arrows indicate primer pairs for the detection of retained introns of SOX9 (n) and SNAI2 (p). q HCR showing detection of retained introns of SOX9 and SNAI2 in embryos transfected with PHF5A gRNA. Dotted lines outline the transverse neural tubes where the “+” indicates the transfected side. Scale bar: 50 μm. Mean ± SD. **: $p < 0.01$, ***: $p < 0.001$.

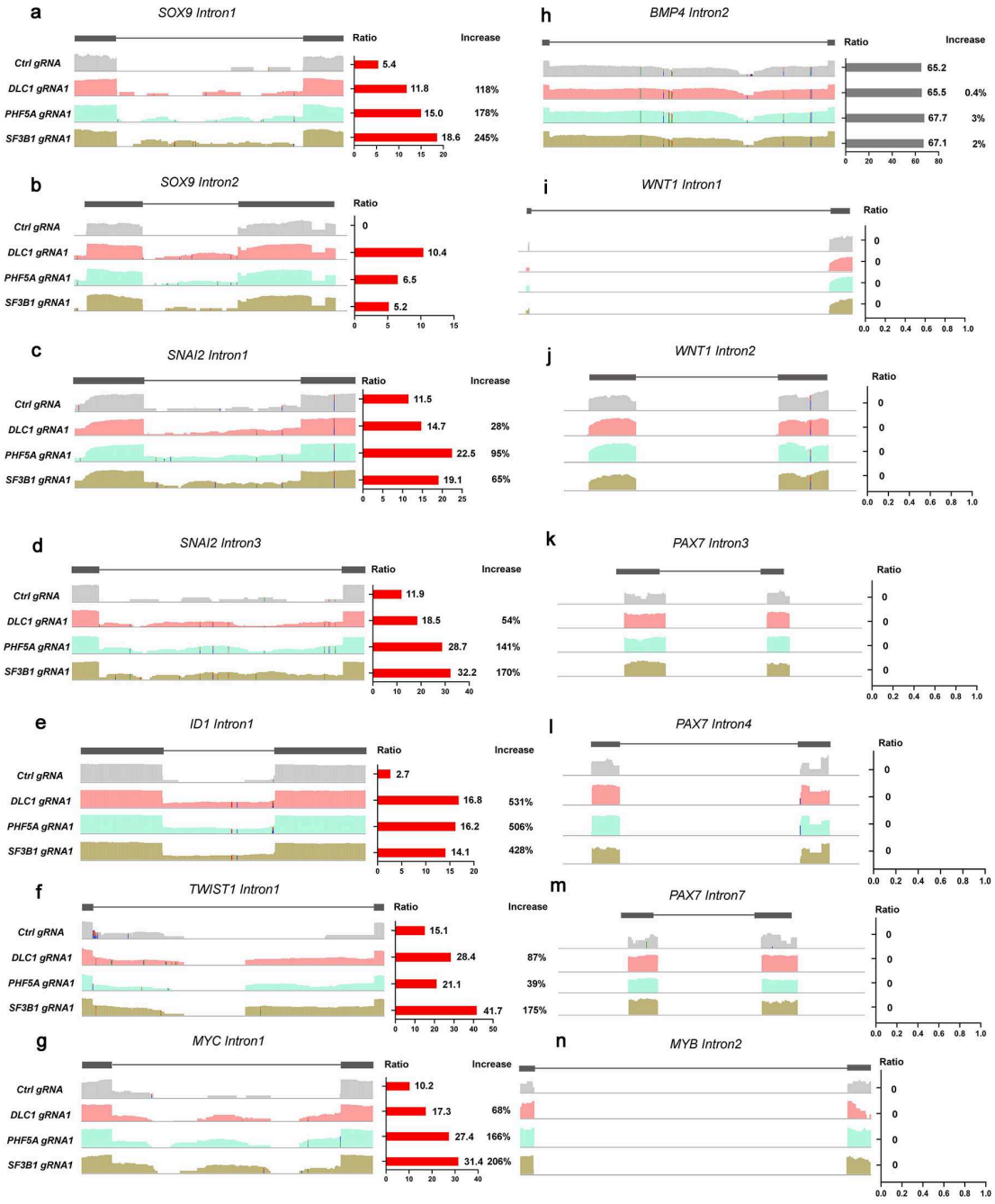


Figure 3

Transcriptomic profiling reveals increased intron retention of NC specifier genes in embryos lacking DLC1, PHF5A, or SF3B1 in the neural tubes. Elevated intron expression levels of SOX9 (a, b), SNAI2 (c, d), ID1 (e), TWIST1 (f), and MYC (g) were detected in the absence of DLC1, PHF5A, or SF3B1 compared to Ctrl gRNA. Intron levels of BMP4 (h), WNT1 (i, j), PAX7 (k, l, m), and MYB (934 n) were unaltered in embryos lacking DLC1, PHF5A, or SF3B1 in the neural tubes.

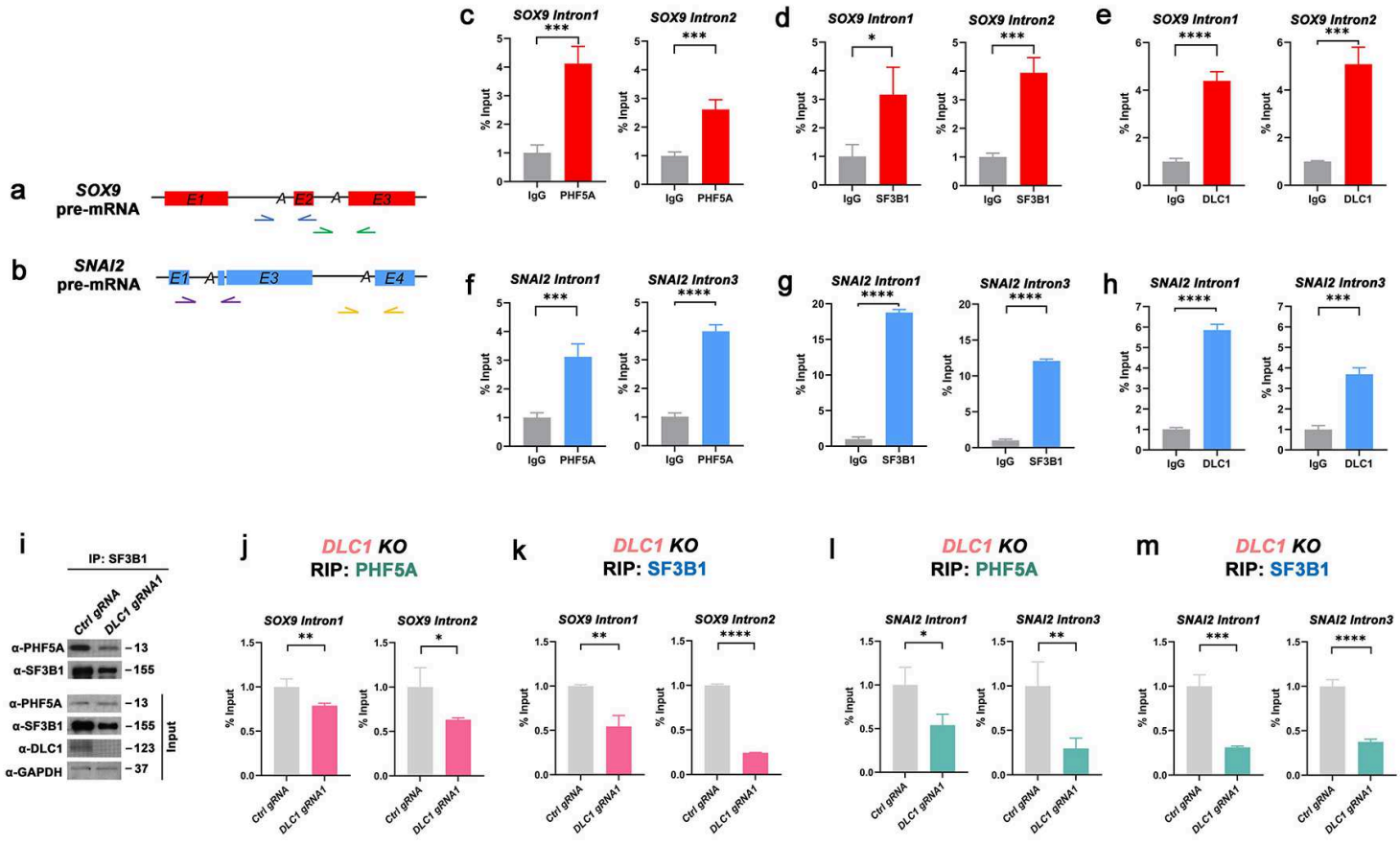


Figure 4

DLC1 is required for the binding of PHF5A and SF3B1 to the introns of NC specifier genes. a, b Schematic diagram shows primer pairs flanking the BPA of SOX9 (a) and SNAI2 (b) introns for RNA-immunoprecipitation qPCR (RIP-qPCR). c to h Graphs show the binding capacity of endogenous PHF5A (c, f), SF3B1 (d, g), and DLC1 (e, h) to the BPA of SOX9 introns 1 and 2 as well as SNAI2 introns 1 and 3 (n=30 per group). (i) IP shows that SF3B1 remained associated with PHF5A in the absence of DLC1. j to m RIP-qPCR analysis reveals reduced binding capacity of PHF5A-SF3B1 splicing complex to introns 1 and 2 of SOX9, as well as introns 1 and 3 of SNAI2 in embryos treated with DLC1 gRNA1 compared to Ctrl gRNA (n=30 per group). Mean ± SD. *: $p < 0.05$, **: $p < 0.01$, ***: $p < 0.001$, ****: $p < 0.0001$

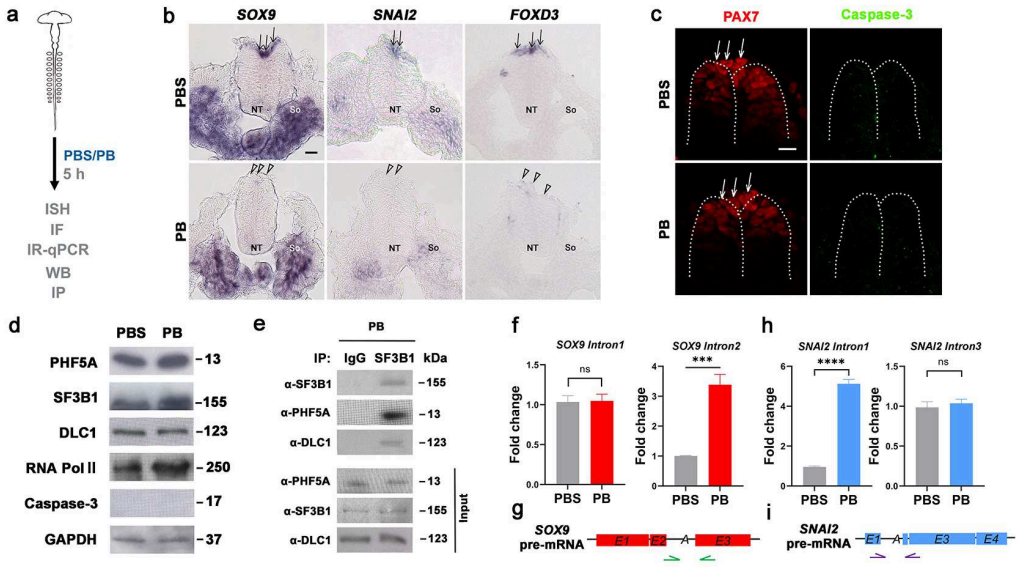


Table 1 Polypyrimidine tract (Py tract) analysis of *SOX9* and *SNAI2* introns

	Gene symbol	Sequence of Py tract at 3' of the branch point adenosine(BPA)	Length	Py tract score	Strength of Py tract
1	*SOX9 Intron1*	ACCGUGUUUUCCCCCCCCUUCCCCAUCCUCC	27 bp	55	strong
2	*SOX9 Intron2*	ACACUCUCUCUUUCCCUU	17 bp	38	weak
3	*SNAI2 Intron1*	AUGUAUCUGUUCC	10 bp	17	weak
4	*SNAI2 Intron3*	AAGCUUGUGCUUCUUUUUU	16 bp	35	strong

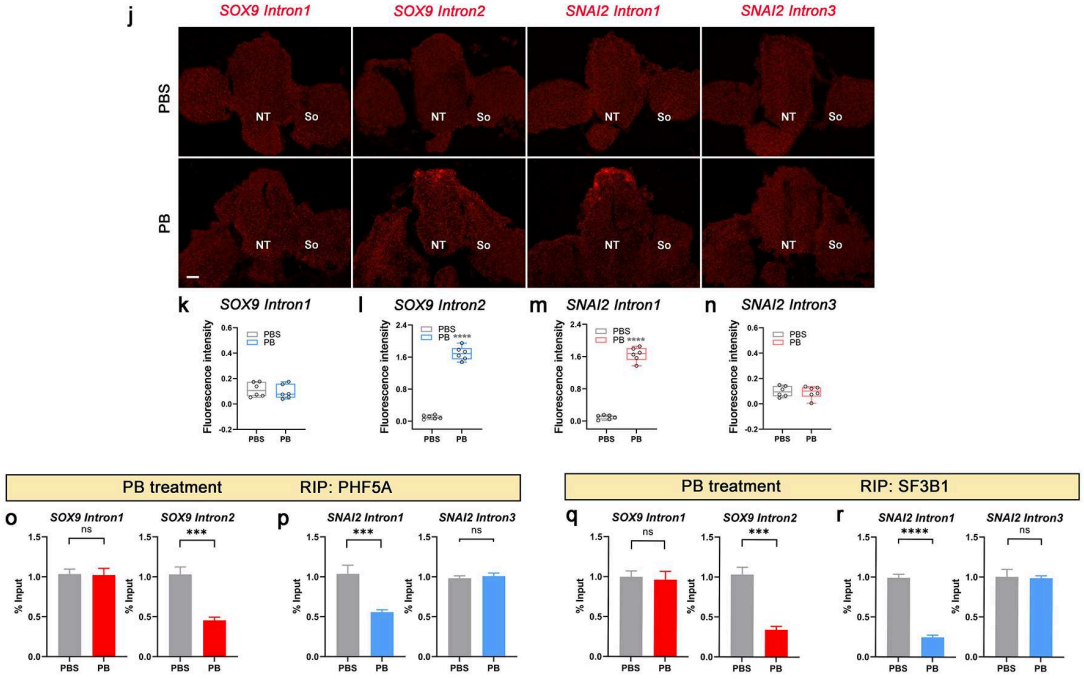


Figure 5

Splicing modulator PB specifically reduces the expression levels of NC specifier genes. a Experimental workflow. b Reduced expression of SOX9, SNAI2, and FOXD3 (open arrowheads) in NCCs of embryos treated with PB, whereas expression of these genes in NCCs (black arrows) and somites (So) remained unaltered in embryos treated with PBS (n=9 per treatment). c PB treatment did not alter the pattern of PAX7 expression (indicated by white arrows) and did not lead to apoptosis, as evidenced by the absence

of Caspase-3+ cells. d PB treatment did not affect the expression levels of PHF5A, SF3B1, DLC1, and RNA Pol II, nor induce Caspase 3 expression compared to PBS Ctrl. e IP analysis revealed that endogenous SF3B1 remained associated with PHF5A and DLC1 in the presence of PB. f and h qPCR data demonstrated increased levels of SOX9 intron 2 (f) and SNAI2 intron 3 (h) in the PB treatment groups compared to the PBS Ctrl. No retention of SOX9 intron 1 and SNAI2 intron 3 was detected in the PB treatment group (n=5 per treatment). g and i Schematic diagrams illustrate the presence of intron 2-retained SOX9 pre961 mRNA (g) and intron 1-retained SNAI2 (i) pre-mRNA after PB treatment. j The HCR analysis revealed the expression of SOX9 intron 2 and SNAI2 intron 1 in NCCs of embryos treated with PB, as compared to the PBS Ctrl. k-n 6 sections per treatment were used for the quantification of fluorescence intensities. o - r PB treatment reduced the binding of PHF5A and SF3B1 on both SOX9 intron 2 (o, q) and SNAI2 intron 1 (p, r) compared to PBS Ctrl. Scale 965 bar: 50 μm. NT, neural tube. Mean ± SD. ***: $p < 0.001$, ****: $p < 0.0001$, ns: no significant difference.

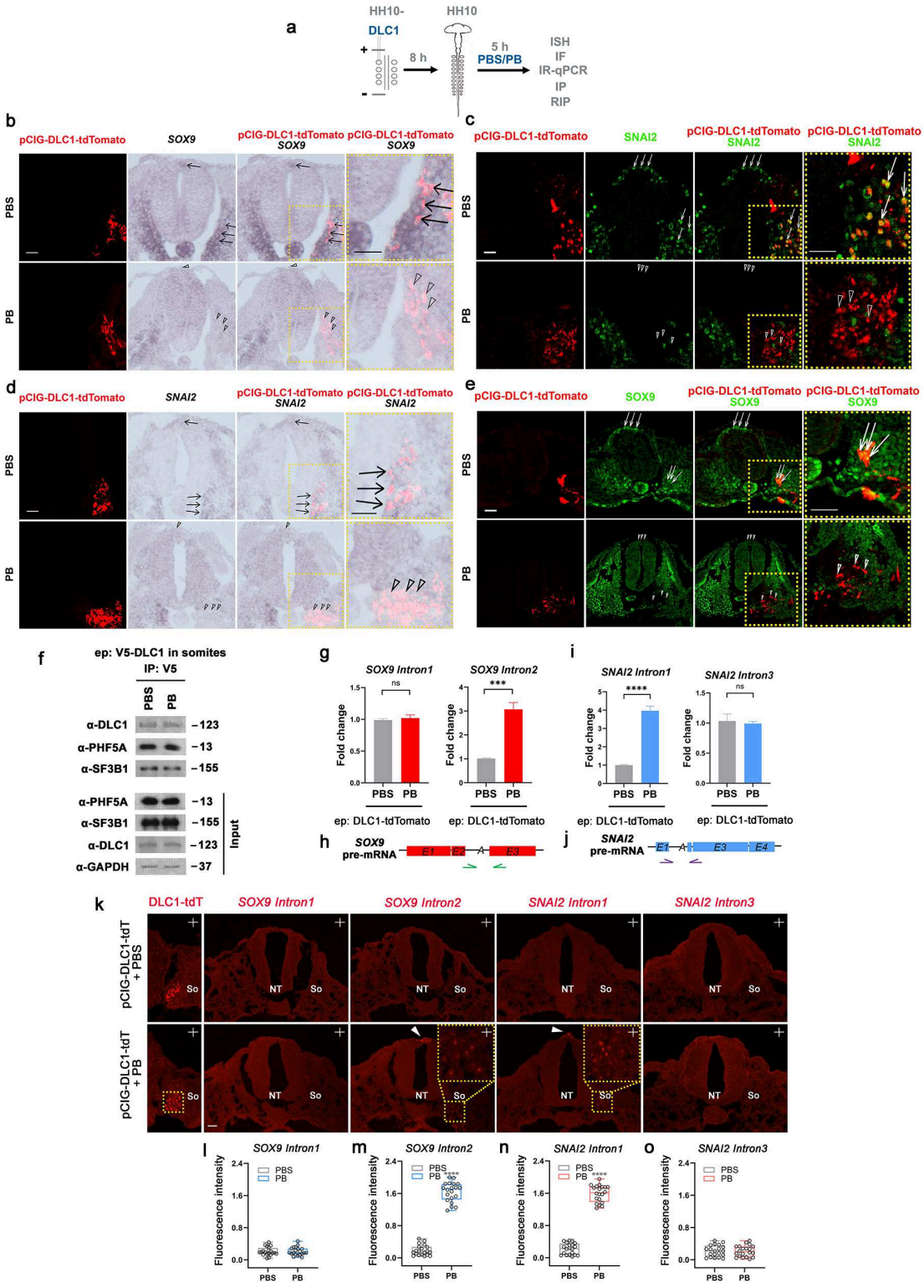


Figure 6

DLC1 determines the increased vulnerability of trunk NCCs to PB treatment. a Experimental workflow. b Ectopic DLC1 expression in somites reduced expression of SOX9 (b, c) and SNAI2 (d, e) in a cell-autonomous manner (open arrowheads) in the PB treatment group. Open arrowheads indicate loss of SOX9 and SNAI2 expression in pre-migratory NCCs. There was no alteration of SOX9 (b, c) and SNAI2 (d, e) expression in DLC1-overexpressing somites and in NCCs (black and white arrows) in the PBS

treatment group. Scale bar, 50 μm. Yellow dotted boxes outline the magnified view in the rightmost column of each panel. f IP shows the association of ectopic DLC1 with endogenous PHF5A and SF3B1 in somites of embryos treated with PBS Ctrl and PB. g and i Electroporation of DLC1 in somites resulted in increased levels of SOX9 intron 2 and SNAI2 intron 1 in the presence of PB compared to PBS Ctrl (n=5 per group). h and j Schematic diagrams depict the presence of intron 2-retained SOX9 pre-mRNA (h) and intron 1-retained SNAI2 pre-mRNA (j) in DLC1 overexpressing somites of embryos treated with PB. k The HCR analysis revealed the expression of SOX9 intron 2 and SNAI2 intron 1 in DLC1-overexpressing somites (So) of embryos treated with PB, as compared to the PBS Ctrl (n=5). l-o 20 sections per treatment were used for the quantification of fluorescence intensities. NT, neural tube. Scale bar: 50 μm. Mean ± SD. ***: $p < 0.001$, ****: $p < 0.0001$, ns: no significant difference.

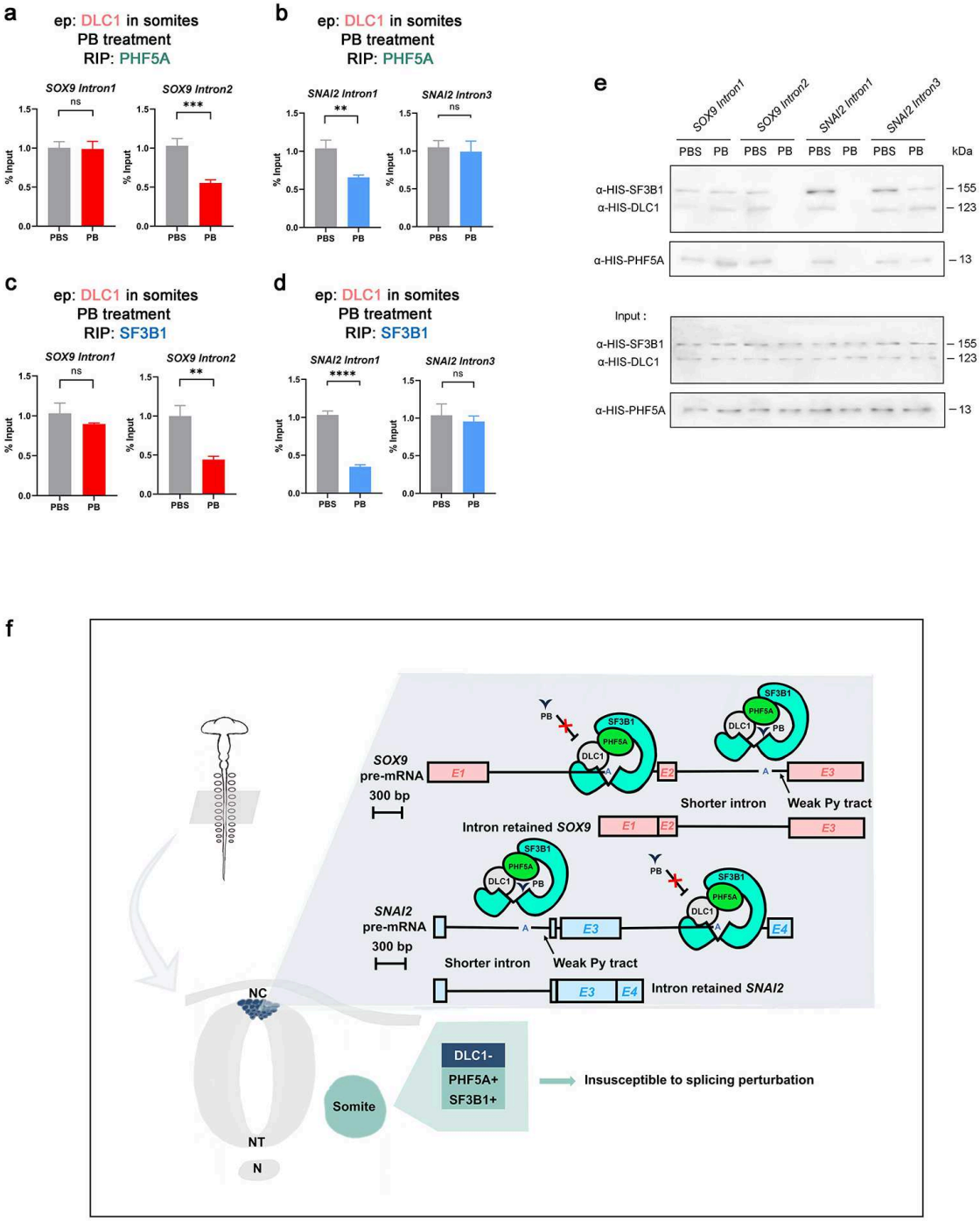


Figure 7

The binding of the DLC1-SF3B1-PHF5A complex to shorter introns of NC specifier genes renders them more susceptible to splicing perturbation by PB a, b Overexpression of DLC1 in somites of embryos treated with PB resulted in reduced binding capacity of PHF5A to SOX9 intron 2 (a) and SNAI2 intron 1 (b) compared to PBS Ctrl. c, d Overexpression of DLC1 in somites of embryos treated with PB led to a reduction in the binding capacity of SF3B1 to SOX9 intron 2 (c) and SNAI2 intron 1 (d) compared to PBS

Ctrl. e In vitro translated SF3B1, DLC1, and PHF5A proteins, each fused with an HIS-tagged, failed to bind to the biotinylated SOX9 intron 2 and SNAI2 intron 1 in the presence of PB. However, PB did not alter the ability of these proteins to bind to the biotinylated SOX9 intron 1 and SNAI2 intron 3. f Schematic diagram depicts the regulation of SOX9 and SNAI2 pre-mRNA splicing in prospective NCCs by the ubiquitously expressed SF3B1-PHF5A splicing factors, in association with NCPage specific DLC1. The DLC1-SF3B1-PHF5A splicing complex plays a 996 crucial role in determining NCC fate and makes them more susceptible to the splicing modulator PB. This susceptibility is due to competitive inhibition of BPA recognition by the complex, which occurs in both SOX9 intron 2 and SNAI2 intron 1 due to their shorter length and weak Py tract, resulting in intron retention and loss of NC progenitors. Mean ± SD. **: $p < 0.01$; ***: $p < 0.001$, ns: no significant difference.

Supplementary Files

This is a list of supplementary files associated with this preprint. Click to download.

- SupplementaryFiglegends.pdf
- DataS1.xlsx
- DataS2.xlsx
- DatasetS120240406.xlsx
- DatasetS220240406.xlsx
- DatasetS320240406.xlsx
- Table1.png